THESIS

ADENOSINE TRIPHOSPHATE IS AN ALLOSTERIC INHIBITOR OF COXSACKIEVIRUS B3 3D^{pol}

Submitted by

Jonathan Paul Karr

Department of Biochemistry and Molecular Biology

In partial fulfillment of the requirements

For the Degree of Master of Science

Colorado State University

Fort Collins, Colorado

Spring 2016

Master's Committeee:

Advisor: Olve Peersen

Robert Cohen
Rushika Perera

ABSTRACT

ADENOSINE TRIPHOSPHATE IS AN ALLOSTERIC INHIBITOR OF COXSACKIEVIRUS B3 $3D^{pol}$

Picornaviruses pose a significant threat to human and animal health, but at present there are no drugs to prevent or treat picornaviral infections. However, intensive study of the picornaviral lifecycle has revealed several promising pharmacological targets, including the RNA-dependent RNA polymerase, $3D^{pol}$, that is responsible for replicating the viral genome. $3D^{pol}$ is central in the virus lifecycle, determines the distribution of mutants in viral progeny, and is a very highly conserved protein across picornavirus species. As such, it is an attractive target for antiviral research. The only $3D^{pol}$ inhibitors that have been found to date are nucleoside analogues that act directly on the active site, even though global dynamics of the protein that are sensitive to allosteric effects of various mutations have been shown to be important determinants of fidelity. The research presented in this thesis provides the first direct evidence of allosteric regulation of $3D^{pol}$ by a small molecule. Inhibition assays investigating the relative affinities of a stalled coxsackievirus elongation complex for non-cognate nucleotides uncovered a mixed inhibition profile of ATP. Among the six picornavirus species tested, this mode of inhibition seems specific to coxsackievirus B3 (CVB3). Engineered mutations in CVB3 $3D^{pol}$, including two that were previously found to lower polymerase fidelity, diminish the uncompetitive component of ATP inhibition. ATP inhibition was found to be dependent on the β- and γ-phosphates. The potential role of ATP's allosteric effect in the virus lifecycle as well as the importance of a biochemically confirmed allosteric site on the polymerase are discussed.

TABLE OF CONTENTS

LIST OF FIGURES

Chapter 1

Introduction

1.1 Picornavirus Background

Viruses of the family *Picornaviridae* comprise an important class of pathogens that continues to take a major toll on human and animal health across the globe.[1] Picornaviruses cause a large variety of diseases with diverse tissue tropism, from the common cold to poliomyelitis to foot-and-mouth-disease.[2] Such diversity is achieved in spite of a small 7.5 to 10 kb genome,[3] a proteome of only eight mature proteins, and a high level of antigenic conservation.[4] Though their adaptability has made picornaviruses difficult to treat and eradicate, the conservation of certain viral proteins provides hope for broad-spectrum antivirals.[5,6] Currently, however, no such antivirals exist, though there have been numerous but ultimately unsuccessful lead compounds targeting different points in the virus lifecycle, especially through inhibition of viral proteins.[6]

Upon infection of a host cell, the viral positive-sense single-stranded RNA (+ssRNA) genome is directly translated by host machinery into a polyprotein that undergoes proteolytic processing to yield structural and nonstructural proteins. The nonstructural 3D protein, dubbed $3D^{pol}$, uses the +ssRNA molecule as a template to synthesize a negative strand intermediate that in turn serves as a template for positive strand synthesis. Early in infection, translation by host proteins is favored by default and mostly suppresses negative strand synthesis. As viral proteins accumulate, they interact with cloverleaf and IRES structures in the 5'-untranslated region of the +ssRNA to suppress translation and promote replication.[7] $3D^{pol}$ then amplifies the genome in

"replication factory" complexes that form on the surfaces of newly synthesized cytoplasmic membranes where replication components are concentrated and the double-stranded RNA intermediate is protected from innate immunity responses.[8]

Since $3D^{pol}$ is central to the replication of the genome, it is likely a crucial determinant of the kinetics of the viral lifecycle, especially in the early stages of infection when viral RNA is limiting. $3D^{pol}$ is also responsible for generating a distribution of mutant genotypes, named quasispecies, by virtue of its relatively low replication fidelity. Genetic diversity of virus populations allows fast adaptation to environmental pressures and is crucial for tissue tropism and pathogenicity. As a result, high-fidelity virus strains are attenuated.[9,10] On the other hand, RNA viruses require a minimum genetic stability and are susceptible to "error catastrophe" if mutation rates exceed wild type rates significantly, causing low-fidelity mutants to also be attenuated.[11,12] Hence, though mutation frequencies among RNA viruses are on the order of a million times higher than what is observed in eukaryotic DNA polymerases,[13,14] they are at a delicate optimum for virulence.[11,15] Modulators of $3D^{pol}$ fidelity therefore have the potential to attenuate picornaviruses.

Because of its central role in virus lifecycle as a fine-tuned determinant of viral fitness, $3D^{pol}$ has been the subject of much research in the last twenty years. A combination of biochemistry, molecular genetics, and structural biology has elucidated the mechanisms of $3D^{pol}$ function and fidelity.[16] Concurrently, antivirals targeting the hepatitis C virus (HCV) RdRp, HIV reverse transcriptase, and herpes virus DNA polymerase have met with success, validating viral nucleic acid polymerases as antiviral targets.[6,17,18] Hence, in the face of a total shortage of drugs against picornaviruses, $3D^{pol}$ should be intensely studied as a potential pharmacological target. After reviewing foregoing research on the polymerase, the work presented in this thesis will

elucidate a potential regulatory mechanism in a subset of picornaviruses that could inform design and discovery of allosteric inhibitors of $3D^{pol}$.

1.2 $3D^{pol}$ Overview

As reviewed by Ferrer-Orta *et al.*, RdRps are structurally homologous to the three other families of nucleic acid polymerases: DNA-dependent DNA polymerases, DNA-dependent RNA polymerases, and reverse transcriptases.[19] They share an overall fold described as a cupped right hand with palm, fingers, and thumb domains that form three important channels intersecting at the active site: the template entry channel, the NTP entry channel, and the product exit channel. However, RdRps are distinct in the structure of their active site. Whereas in the other classes of nucleotide polymerases flexibility of the fingers domain allows for dramatic swinging motions responsible for active site closure, the RdRp fingers domain makes inflexible contact with the thumb domain via an extended loop, permanently encircling the active site.[20]

Due to their "closed hand" configuration, RdRps have a different mechanism to structure the active site for catalysis. $3D^{pol}$ uses a hydrogen-bonding network between the 2'- and 3'-hydroxyls of the incoming nucleotide with palm-domain residues to trigger active site closure via structuring a three-stranded β-sheet in the palm domain.[20] This positions two divalent cations coordinated by conserved aspartate residues in the palm domain proximal to the α-β phosphodiester-linkage of the incoming nucleotide, where they catalyze nucleophilic attack by the 3'-OH of the priming nucleotide. Catalysis requires the coordinated action of a conserved lysine in the palm domain to act as a general acid to protonate the pyrophosphate leaving group.[21] Together these findings reveal an important feature of RdRps: recognition of the incoming nucleotide via interactions with its sugar and triphosphate moieties is coupled to active site closure and subsequent catalysis.[20] That substrate recognition (quantitated as a K_d) and the

committed step of catalysis (limiting k_{cat}) are one event facilitated by the coordinated motions of a single domain helps explain why speed and fidelity are negatively correlated in $3D^{pol}$,[22] because fast active site closure can compensate for weak binding per the catalytic efficiency ($k_{spec}=k_{cat}/K_d$). That discrimination depends on the orientation of the ribose hydroxyls explains the experimental convenience that *in vitro* discrimination factors for incorporating 2'-deoxy nucleotides are predictive of *in vivo* misincorporation rates.[11,22]

Owing to the palm domain's central role in catalysis, it is unsurprising that it contains five of the eight conserved polymerase motifs (A-E)[23] and that most known mutations of $3D^{pol}$ that modulate fidelity are within this domain.[11,22,24] Unexpectedly, though, the two characterized mutations with the most dramatic effects on poliovirus $3D^{pol}$ fidelity, the high-fidelity G64S and low-fidelity H273R mutations, reside in the fingers domain more than 15 Å away from the active site.[25] This implicates long-range interaction networks as important contributors to fidelity.[26] Molecular dynamics and NMR studies have confirmed that global dynamics of $3D^{pol}$ determine the binding competency of the active site for incoming nucleotide and that dynamics of the palm domain depend on the correctness of the incoming nucleotide, directly affecting catalytic efficiency.[27,25,28] It is also known that native packing of the N-terminus distal to the active site is necessary for elongation activity,[29,30] providing additional evidence for a tight network of interactions collaborating throughout the polymerase to facilitate function.

1.3 $3D^{pol}$ Enzymatic Mechanism

In order to understand and manipulate $3D^{pol}$ fidelity, the polymerase's mechanism of catalysis has been thoroughly investigated from both biochemical and structural angles. These studies have elucidated the steps in the chemical cycle of $3D^{pol}$ as well as the key residues and

structural motifs whose coordinated actions facilitate its function. Together, their findings paint an almost complete picture of the mechanistic basis of polymerase fidelity.

The full catalytic cycle of poliovirus $3D^{pol}$ was biochemically characterized by Arnold and Cameron and was found to be highly similar to already known nucleic acid polymerase mechanisms.[31] Beginning from an enzyme-RNA complex, the sequence of enzymatic events is binding of an NTP to form a ternary complex, a conformational change into a catalytically competent state, phosphoryl transfer (NMP incorporation), a second conformational change, and finally release of pyrophosphate to regenerate the original state. All steps up to and including catalysis were found to be isoenergetic, with both the first conformational change and phosphoryl transfer being partially rate-limiting. Post-catalysis, the RNA must translocate to move the next templating base adjacent to the active site. While the chemical assays used in this study were not sensitive to translocation *per se*, the authors suggest that the second conformational change is translocation because this step is essentially irreversible due to the large ΔG (-7.3 kcal/mol) driving it forward. Though pyrophosphate release was placed after translocation in their model, the authors note that a pre-translocation conformational change that allows pyrophosphate release could also explain the data.

Gong and Peersen complemented the biochemical approach with crystallographic studies.[20,32] By crystallizing poliovirus elongation complexes, they were able to capture four distinct states that likely represent intermediates in the catalytic cycle, leading to a structural model in good agreement with the previous one. Before binding an NTP, the templating base is prepositioned in the active site and fully stacked on the upstream nucleotide. Upon binding, the incoming nucleotide base-pairs with the templating base and stacks on the priming nucleotide. It was observed that in the absence of either the 2'- or the 3'-hydroxyl on the NTP ribose, the NTP

could bind and cause subtle rearrangements in the fingers domain, but a catalytically competent state was not observed; rather, the triphosphate was 1 Å too distant from the active site, no divalent metals were coordinated, and the palm domain remained unstructured. In this state, the active site was said to be open. When the fully cognate nucleotide is present, motif A forms a three-stranded β-sheet with motif C, two Mg^{2+} ions are coordinated by Asp233, and the extensive hydrogen-bonding network between the palm domain and the ribose hydroxyls brings the triphosphate into close proximity to the catalytic residues. The authors dubbed this the closed conformation, which is catalytically active.

Interestingly, a post-catalysis relaxation back to the open state occurred without translocation, indicating that the two events are not necessarily coupled. This led to the addition of a sixth step in the catalytic cycle, a pre-translocation opening of the active site followed by release of pyrophosphate (see Figure 1.1). This allows for the possibility of pyrophosphate release being the trigger for translocation, which has been suggested as a general mechanism for polynucleotide polymerases.[33] (For further discussion of translocation, see Section 3.4.2.)

Finding that palm domain dynamics are principally responsible for closing the active site inspired the design of numerous mutations in CVB3 $3D^{pol}$ to attenuate viral replication.[11,22] Virology studies showed that several palm domain mutants were stable and exhibited a mutator phenotype and that the *in vivo* mutation rates had a negative correlation with the polymerase's ability to discriminate between 2'-deoxyCTP (dCTP) and CTP *in vitro*. Of these, the motif A mutants I230F and F232Y had the most dramatic phenotype and lowest discrimination factor. These two mutants did not have a significantly altered K_d for CTP, which is to say that they did not have a direct effect on nucleotide recognition. Rather, they had a faster maximum elongation rate by >20%, suggesting that active site closure rather than nucleotide binding is the fidelity

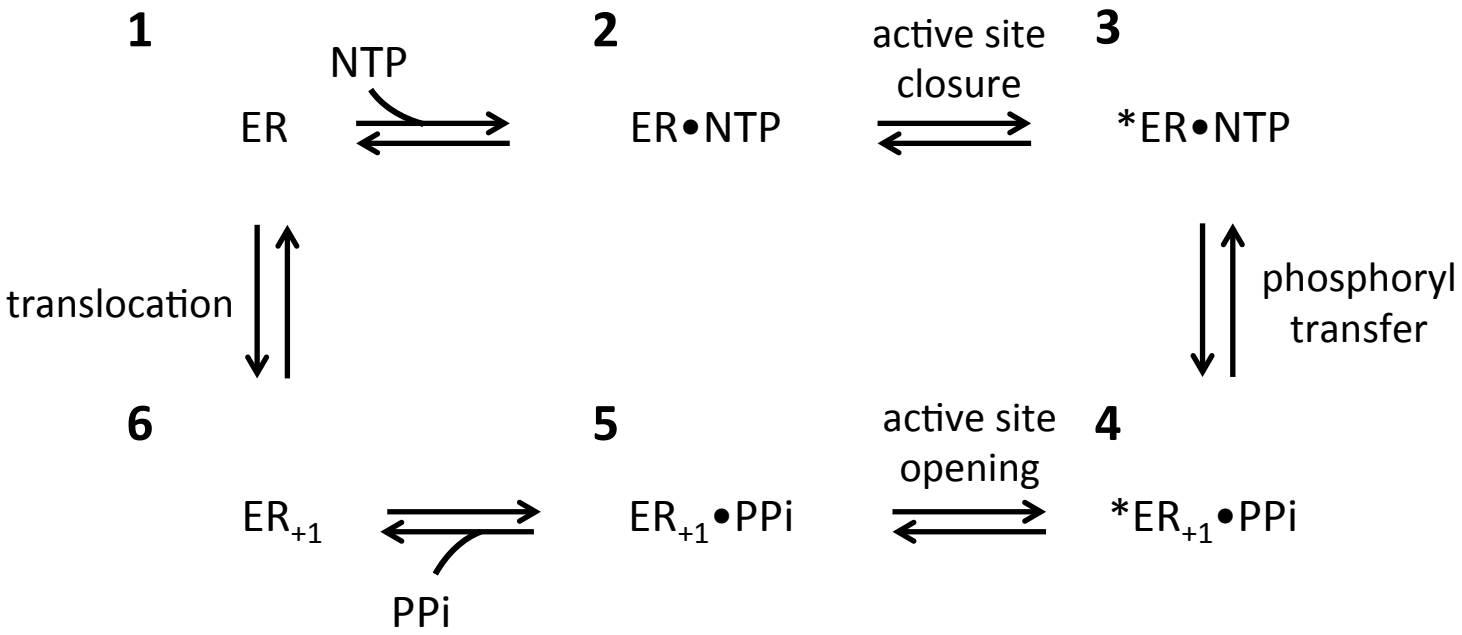

FIG 1.1 Six-state model of 3D^{pol} catalytic cycle. Combined model from structural and biochemical studies.

checkpoint these mutants bypass. Since the 230 and 232 residues are not in the active site, these mutations must decrease polymerase fidelity by disrupting the structure and dynamics of motif A and thereby indirectly impact catalytic efficiency. This provides further evidence that dynamic restructuring of the palm domain is needed for active site closure and that such dynamics are at least partly dictated by residues distant from the active site.

1.4 Allostery in $3D^{pol}$

That polymerase dynamics, especially in the palm domain, play a role in determining polymerase fidelity provides hope for the development of allosteric regulators since allostery is known to work primarily through dynamic rather than static structural effects.[34] Allosteric regulators of $3D^{pol}$ therefore have potential as prophylactics as well as therapeutics because they could attenuate picornaviruses by perturbing their delicate optimum between speed and fidelity.

Furthermore, allosteric regulators potentially avoid the shortcomings of the other class of $3D^{pol}$ inhibitors, nucleotide analogues. As discussed by Graci *et al.*, the more direct strategy of using nucleotide analogues as chain terminators to arrest elongation or as mutagens to induce error catastrophe has encountered significant roadblocks.[35] The first barrier to this class of compounds is delivery to the cytoplasm since phosphates prohibit transmembrane diffusion. Using nucleoside analogues (such as the adenine/guanosine analogue ribavirin) partially circumvents this problem since some have a limited ability to passively diffuse through membranes and many can enter through nucleoside transporters present on almost all cell types. However, the transporters' specificity and size restraints restrict what substituents can be added to modify the drug. Once inside the cell, the nucleoside must be a substrate of multiple kinases to become a mutagenic NTP and at the same time avoid being a substrate for ribonucleotide reductases that could make it a mutagenic dNTP. Of course, it also must be a substrate for $3D^{pol}$.

Finally, it must do all of the above without disrupting the exquisitely regulated nucleoside metabolism pathways, which could be the limiting factor of ribavirin's usefulness.[36] These difficulties with using nucleoside analogues as therapeutics underscore the usefulness of small-molecule allosteric regulators in modulating polymerase fidelity.

There is only one site on the surface of $3D^{pol}$ known to have allosteric properties. Interface I was identified in the first X-ray crystal structure of poliovirus $3D^{pol}$ as a contact between the thumb domain of one polymerase and the fingers domain of another. Because of its large surface area (1480 $Å^2$ total) and very specific contacts, it was proposed to be a real and important interface, not just a crystallographic artifact.[37] It has since been shown to mediate oligomerization of $3D^{pol}$ into membrane-associated arrays both *in vitro* and *in vivo*, potentially promoting RNA binding and elongation through allosteric effects.[38,39] Additionally, disrupting Interface I has been shown to hamper the uridylation of the viral VPg protein that serves as a primer for RNA synthesis, perhaps through disrupting binding of 3CD to $3D^{pol}$ or through allosteric effects within $3D^{pol}$ itself.[40,41] Interface I could therefore be a potential target for allosteric regulators, but because of its size it may be better fit for protein rather than small molecule ligands.

The research detailed in the following chapters uncovers a novel allosteric regulation of $3D^{pol}$ elongation by ATP at cellular concentrations. Mutations that disrupt this behavior are characterized and may indicate where on the polymerase ATP is binding. Additionally, computational methods are employed to identify potential allosteric sites. The potential role of ATP's allosteric effect in the virus lifecycle as well as the importance of a confirmed allosteric site on the polymerase are discussed.

Chapter 2

Kinetic Studies of NTP Inhibition of $3D^{pol}$

2.1 Introduction

In the context of a host cell, $3D^{pol}$ must discriminate between all four NTPs as it replicates the viral genome. Its fidelity is dictated by the efficiency with which it incorporates the cognate nucleotide over non-cognate nucleotides. This efficiency can be quantitated as the quotient of two kinetic parameters, the rate of incorporation (k_{cat}) over the effective affinity for the nucleotide (K_d^{app}). The relative affinities of the enzyme-RNA complex for the respective nucleotides are therefore a significant contributor to fidelity, and, along with corresponding rates of incorporation, dictate the rates of misincorporation and thus which misincorporations are more likely.[42] Indeed, the competitive inhibitor constant (K_{ic}), which describes the complex's affinity for the inhibitor species, is equivalent to the Michaelis constant (K_m) for that species as an alternate substrate.[43] Hence, a mutant that differentially affects the polymerase's affinities and incorporation rates for different nucleotides has the potential to modulate fidelity, not only in how many misincorporations are made but also in the frequencies at which different misincorporations occur. Measurement of inhibition constants could therefore be another *in vitro* tool to characterize fidelity.

The research presented in this chapter uses stopped-flow kinetics to probe the inhibitory effects of non-cognate NTPs on the incorporation of CTP in a fluorescent single-turnover system. Several picornaviral polymerases, including a series of engineered mutations in coxsackievirus B3 (CVB3) polymerase, are examined. Unexpectedly, ATP is found to be a

mixed inhibitor of CVB3 $3D^{pol}$. Further experiments as well as the analysis in the next chapter were performed in an effort to characterize the uncompetitive component of ATP inhibition, including attempts to locate its allosteric binding site on the polymerase surface.

2.2 Materials and Methods

2.2.1 Mutagenesis, Protein Expression, Purification

Site-directed mutagenesis was performed using the QuikChange protocol (Agilent, CA) and confirmed through sequencing by Genewiz, Inc. Protein constructs were expressed and purified as described previously in [44].

2.2.2 Fluorescence

Kinetic experiments employed a fluorescent RNA (see Figure 2.1), named a polymerase elongation template element (PETE), that recapitulates primer-template duplex and can facilitate polymerase elongation.[44] After incorporation of a few nucleotides, the elongation complex (EC) stalls and remains very stable with a half-life of several hours. At saturating polymerase concentrations, this setup allows for essentially all the RNA in the system to be bound in the same state at a defined position along the PETE, depending on which nucleotides have been provided. Upon addition of the remaining nucleotide(s), reinitiation and elongation rapidly occur in a synchronized manner, resulting in an exponential fluorescence trace.

The fluorophore that was employed was 2-aminopurine (2AP), a fluorescent adenosine analogue that is highly sensitive to environmental changes, especially base-stacking, which quenches its fluorescence.[45] Incorporating 2AP into the template strand of the PETE allows observation of translocation as the bases downstream of the active site undergo dramatic changes in base-stacking: the base in the +3 position is somewhat stacked on the +4 base, the +2 base is fully unstacked, and one face of the +1 base is stacked on the upstream duplex (Figure 2.1). As

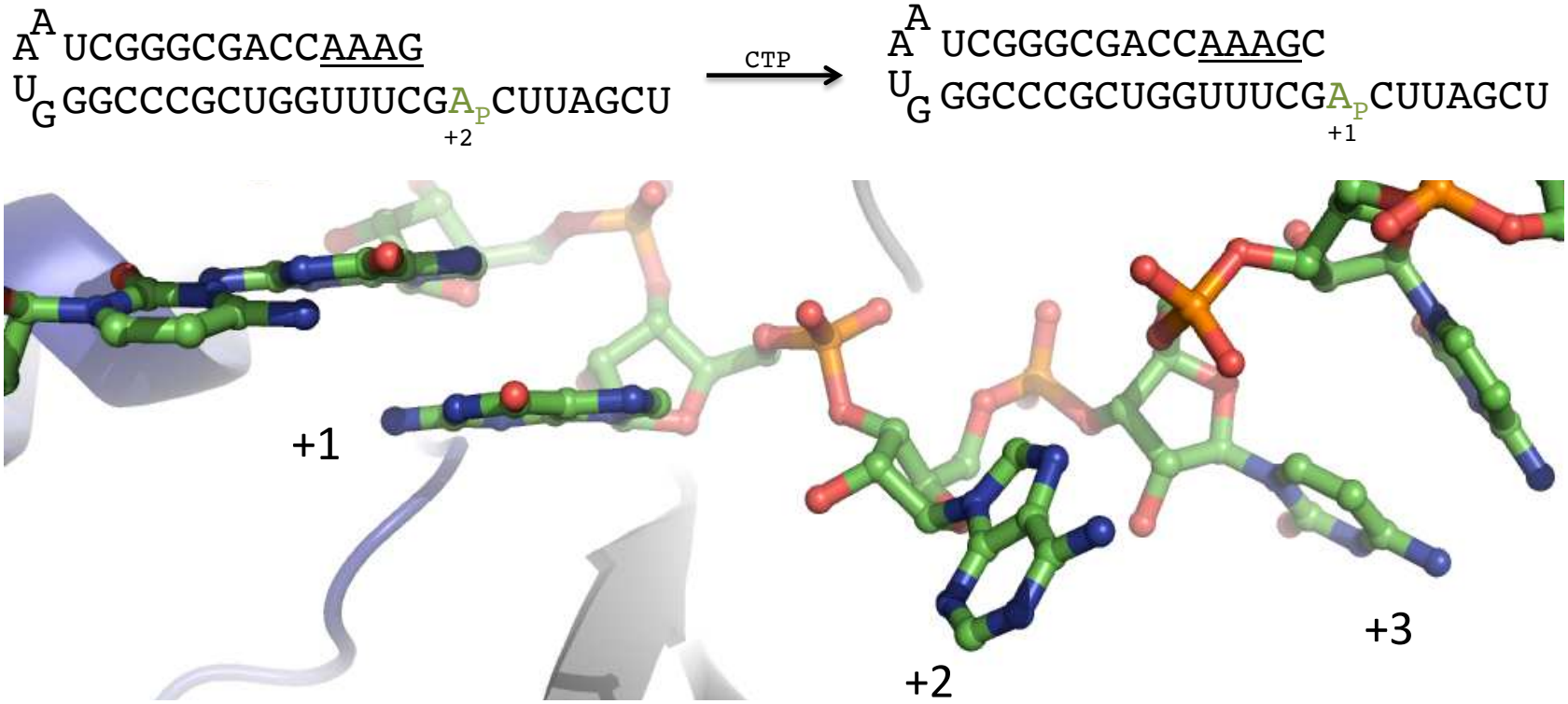

FIG 2.1 Molecular basis of PETE 2AP fluorescence change. *Above:* Fluorescent PETE used in elongation assays showing where the polymerase stalls after incorporating AMP and GMP (underlined). Before CMP incorporation, the templating base in the +1 position is guanidine and 2-aminopurine (green) is in the +2 position. Incorporation of CMP and subsequent translocation move 2AP into the +1 position. *Below:* Elongation complex structure showing the extent of stacking in the base positions immediately downstream of duplex RNA (PDB: 4K4Y).

2AP moves through these positions, there is first a large increase in fluorescence ($+3 \rightarrow +2$) and then an even larger decrease ($+2 \rightarrow +1$). By mixing complex with nucleotides in a rapid-mixing stopped-flow instrument, kinetic parameters can be extracted from 2AP fluorescence traces. It should be noted that, in this system, k_{pol} is an apparent rate since it includes multiple steps and reports on the rate-limiting step, which is most likely active site closure and not catalysis.[22] Since this is a single-turnover experiment, the hyperbolic dependence of rate on substrate concentration is an apparent K_d, not a K_m.[46]

2.2.3 Elongation Complex Assembly

Elongation complexes were assembled at final concentrations of 30 μM $3D^{pol}$, 10 μM PETE RNA, 112 mM NaCl, 2 mM HEPES pH 7, 4 mM $MgCl_2$, 5 mM TCEP. 60 μM each of ATP and GTP was added and the reaction was incubated for 30 minutes at room temperature to pause the complex with a templating guanosine in the +1 position and 2AP in the maximally fluorescent +2 position (see Figure 2.1). This reaction was then diluted 200-fold in reaction buffer (75 mM NaCl, 2 mM HEPES pH 7, 4 mM $MgCl_2$) and used in stopped-flow experiments at a final EC concentration of 12.5 nM.

2.2.4 Stopped-Flow Experiments

All solutions used in stopped-flow experiments were in reaction buffer. All NTP solutions were prepared with $MgCl_2$ so that the Mg^{2+} concentration was always in 4 mM excess over final NTP concentration. Elongation reactions were carried out in a Bio-Logic SFM-4000 titrating stopped-flow instrument with an MOS-500 spectrometer at 30°C. Fluorescence excitation was at 313 nm with a 10 nm bandwidth and emission was detected using a 370/36 nm band pass filter.

2.2.5 Graphical Analysis

Fluorescence traces were fit to either a double exponential ($b + A_1e^{-k_1t} + A_2e^{-k_2t}$) or double exponential with a linear ($b + A_1e^{-k_1t} + A_2e^{-k_2t} + k_3t$) using Kaleidagraph (Synergy Software). The rate of the dominant exponential was used in subsequent linear plots.

Calculations of inhibition constants were made using Dixon and Cornish-Bowden linearization plots.[47,48] Both analyses are based on the Michaelis-Menten equation, which in its expanded form is:

$$\textbf{(1)} \quad v = \frac{V_{\max} s}{K_m\left[1 + \frac{i}{K_{ic}}\right] + s\left[1 + \frac{i}{K_{iu}}\right]}$$

where v is the rate, V_{max} is the limiting rate, K_m is the Michaelis constant, K_{ic} is the competitive inhibitor constant, K_{iu} is the uncompetitive inhibitor constant, s is substrate concentration, and i is inhibitor concentration. More specifically, to avoid the hyperbolic nature of the Michaelis-Menten equation, both analyses use the inverse of **(1)**:

$$\textbf{(2)} \quad \frac{s}{v} = \frac{K_m}{V_{\max}}\left[1 + \frac{i}{K_{ic}}\right] + \frac{s}{V_{\max}}\left[1 + \frac{i}{K_{iu}}\right]$$

The Dixon analysis plots the inverse rate versus inhibitor concentration, which rearranges **(2)** to the following:

$$\textbf{(3)} \quad \frac{1}{v} = \frac{K_m}{V_{\max} s}\left[1 + \frac{i}{K_{ic}}\right] + \frac{1}{V_{\max}}\left[1 + \frac{i}{K_{iu}}\right]$$

In this case, two lines representing experiments conducted with different substrate concentrations satisfy the following at the point of their intersection:

$$\textbf{(4)} \quad \frac{1}{s_1}\left[1 + \frac{i}{K_{ic}}\right] = \frac{1}{s_2}\left[1 + \frac{i}{K_{ic}}\right]$$

They can therefore intersect only when $s_1 = s_2$ or $i = -K_{ic}$. Hence, the point of intersection between different lines on a Dixon plot gives the numeric value of K_{ic}, regardless of the uncompetitive term. If the lines are parallel in this plot then no competitive inhibition is present.

The Cornish-Bowden analysis complements that of Dixon by plotting substrate concentration over rate versus inhibitor concentration as suggested by **(2)**. It is easily shown that the intersection of two lines of different substrate concentrations on this plot must satisfy:

$$\textbf{(5)} \quad s_1\left[1+\frac{i}{K_{iu}}\right] = s_2\left[1+\frac{i}{K_{iu}}\right]$$

where the competitive term falls out and the x-coordinate of the point of intersection is equal to the numeric value of $-K_{iu}$. If the lines are parallel in this plot, then no uncompetitive inhibition is present. By using both plots, the mode of inhibition can be clearly diagnosed and the inhibition constants that reflect inhibitor binding constants can be calculated.

Inhibitor constants were calculated by performing a global fit in Graphpad Prism 6.0 (La Jolla, CA) in which all linear fits were constrained to share a common x,y coordinate pair that reflects the intersection point.

2.2.6 Kinetic Modeling

The overall model that was input to fit stopped-flow datasets is schematized in Figure 2.2. The center species, ER4, represents the enzyme-RNA complex that has stalled after four NMP incorporation steps. At this point, all four NTPs compete for the active site, with CTP-binding being the lone productive pathway. All NTP on-rates were assumed to be equivalent while their off-rates were allowed to vary. Both before and after CTP binding, ATP can bind uncompetitively to the allosteric site, resulting in a doubly liganded ER4CA complex that has a reduced rate of CTP incorporation. Catalysis and translocation result in an intermediate (ER5*) that then relaxes to another stalled complex (ER5). This intermediate step was needed to

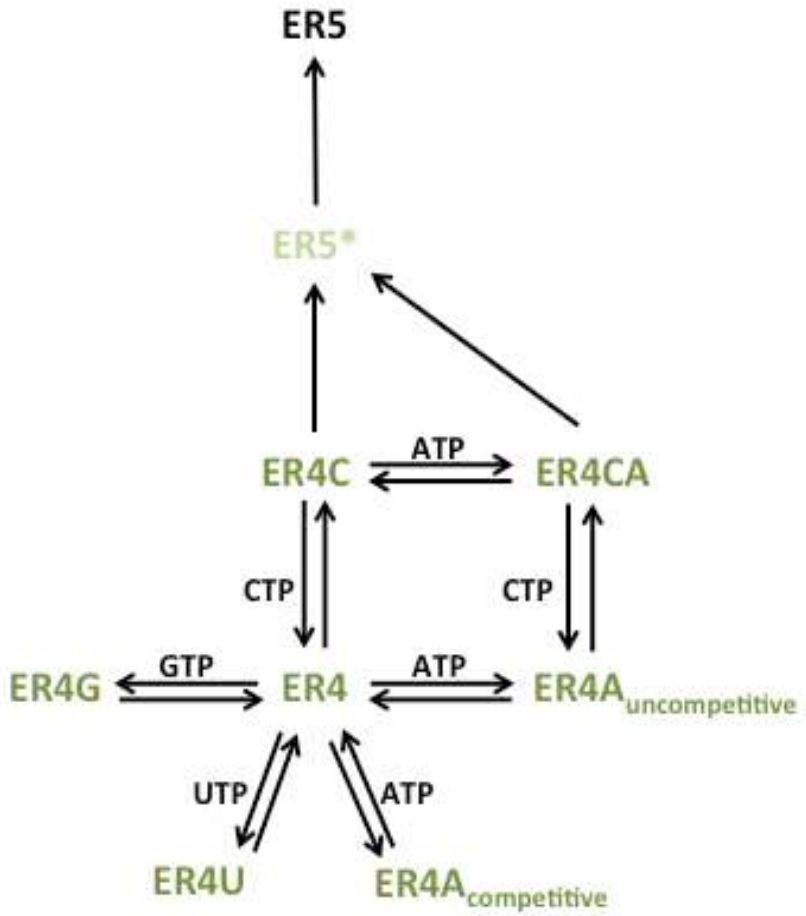

FIG 2.2 KinTek input model of NTP inhibition of CVB3 3D^{pol}. The vertical path from the enzyme-RNA complex after the 4 preparatory incorporations, the ER4 species, models catalysis as a three-step process beginning with binding CTP, followed by incorporation and translocation, and then a relaxation event. All ER4 species are colored green to represent their high fluorescence. ER5* has a 10-fold dimmer fluorescence and ER5 has no fluorescence. Double arrows indicate equilibria, single arrows irreversible events.

accommodate a linear tail in the data (see below). Both catalysis and relaxation are assumed irreversible on the time-scale of these experiments (≤10 seconds).

The single-incorporation fluorescence traces observed in this system are best fit to a double exponential plus a linear component, with the amplitude of the first exponential approximately ten times that of the second. Therefore, the model included three sets of observables: all ER4 complexes, ER5*, and ER5, with the relative fluorescences at a ratio of 10:1:0 respectively. Total fluorescence was allowed to vary between experiments.

2.3 Results

2.3.1 Inhibition of CTP Incorporation by NTPs

To quantitate inhibition of CTP incorporation by non-cognate NTPs in CVB3 $3D^{pol}$, stopped-flow experiments were conducted in which inhibitors were titrated from ~200 uM to ~2 mM against 3-4 constant CTP concentrations near $K_{d(CTP)}$. Quenching of 2AP fluorescence upon addition of CTP results in an exponential curve whose rate is dictated by a pseudo first-order rate constant k_{pol}. Slowing of k_{pol} by an inhibitor can be clearly seen when the fluorescence traces from a titration experiment are plotted against time on a normalized axis (Figure 2.3). An additional exponential term and sometimes a linear term were needed to accurately fit the curves using regression analysis, but since their respective rates did not titrate with inhibitor concentration, they did not factor into the analysis.

Inverse rates as a function of inhibitor concentration were plotted on the single-reciprocal Dixon and Cornish-Bowden plots (Figure 2.3). A series of four titrations against different CTP concentrations showed a clear point of intersection for GTP on the Dixon plot with a $K_{ic(GTP)}$ of 440 uM, which is on order with the physiological concentration of GTP of 300 uM.[49] That the titration lines were parallel in the Cornish-Bowden plot indicates there was no uncompetitive

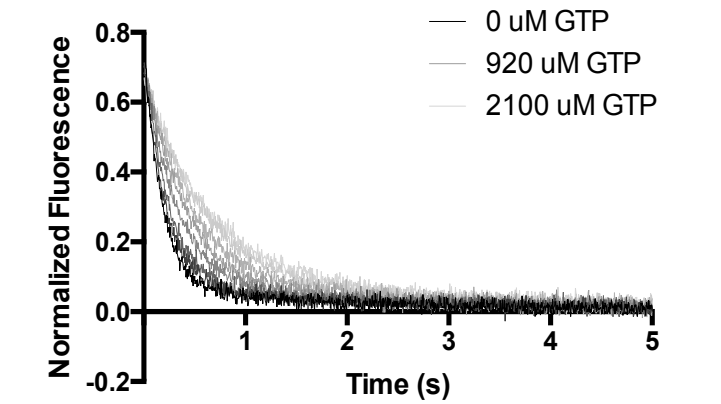

NTP	K_{ic} (uM)	95% Confidence Limits Lower, Upper	K_{iu}
GTP	440	370, 600	N/A
UTP	2900	2200, 6700	N/A

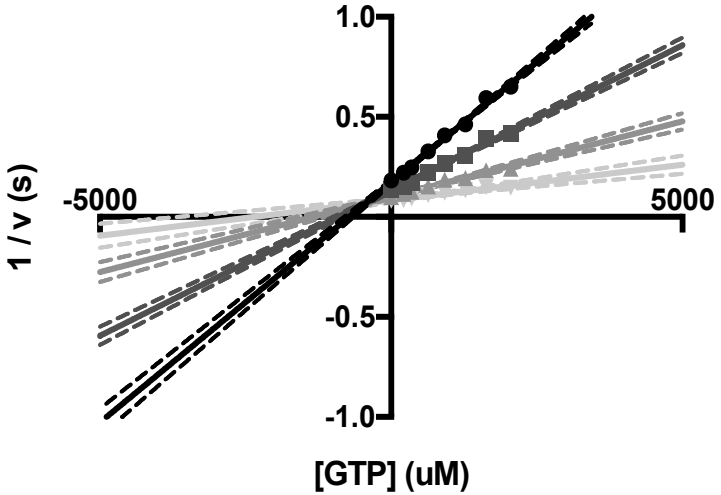

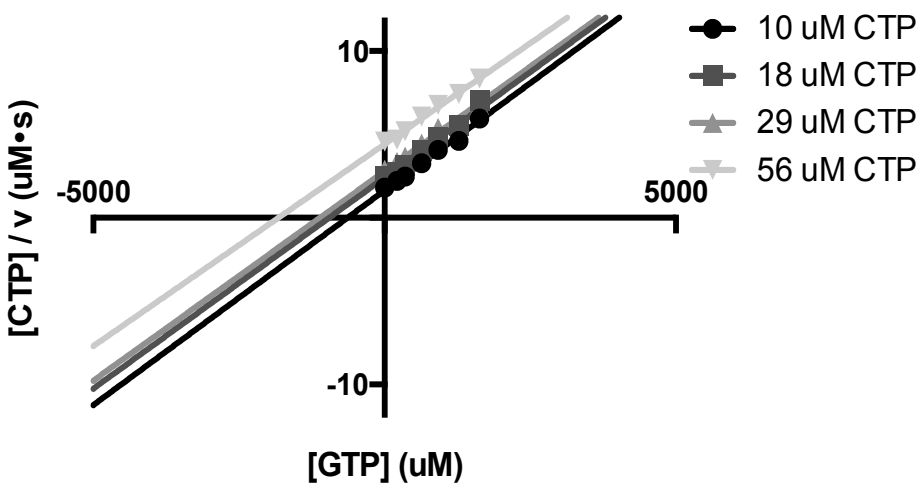

FIG 2.3 GTP and UTP are competitive inhibitors of CTP incorporation. *Upper left*: Representative fluorescence traces from a GTP titration against a constant CTP concentration. *Lower panel*: Dixon (*left*) and Cornish-Bowden (*right*) plots of GTP titrations against four CTP concentrations. Dashed lines represent 95% confidence intervals from fitting the intersection. *Upper right*: Results of global fitting analysis of the single reciprocal plots.

inhibition term. A similar analysis of UTP showed purely competitive inhibition with a $K_{ic(UTP)}$ of 2.9 mM, which is about ten-fold higher than physiological concentrations of UTP of 250 uM.[49]

2.3.2 ATP is a Mixed Inhibitor of CVB3 3D^{pol}

Titration experiments with ATP as the inhibitor revealed a unique inhibition profile. Michaelis-Menten plots showed significant inhibitory effects by ATP on both k_{pol} and $K_{d(CTP)}$ (Figure 2.4), suggesting that ATP is not a purely competitive inhibitor. The Dixon plot of four ATP titrations gave a $K_{ic(ATP)}$ of 1.5 mM and the Cornish-Bowden plot showed a clear intercept at [ATP] = -1.9 mM, indicating that ATP is a mixed inhibitor of CVB3 3D^{pol}. Both $K_{ic(ATP)}$ and $K_{iu(ATP)}$ are a little below the estimated physiological ATP concentration of 2.1 mM.[49]

2.3.3 ATP Inhibition is Phosphate-Driven

To parse which components of ATP are necessary for its inhibitory effects, titration experiments were performed with ADP and AMP (Figure 2.5). ADP had a mixed inhibition profile, with competitive and uncompetitive inhibition constants significantly reduced compared to ATP. Interestingly, the effect on K_{iu} was greater than that on K_{ic}. AMP competitive inhibition was six-fold weaker than that of ATP, with an even weaker uncompetitive component. These results indicate that allosteric ATP binding to the polymerase depends largely on the triphosphate moiety, especially the β-phosphate, without which inhibition is essentially abolished.

2.3.4 ATP Uncompetitive Inhibition is Reduced in Motif A Mutants

Polymerase mutants with known fidelity effects were employed in kinetic experiments to test for altered inhibition by ATP and GTP (since there was not strong inhibition by UTP, it was not used in subsequent experiments). Motif A mutants I230F and F232Y were previously found to have significantly reduced fidelity and increased k_{pol}.[22] Neither had a significantly different

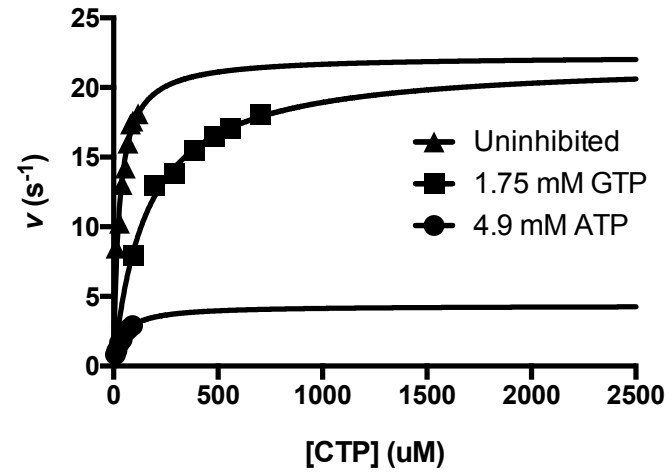

Parameter	Observed (uM)	95% Confidence Limits Lower, Upper	Calculated
$K_{d(CTP)}$	20	17, 23	
$K_{d(CTP)}$ (+GTP)	160	110, 200	
$K_{d(CTP)}$ (+ATP)	45	32, 59	23
V_{max}	18	17, 19	
V_{max} (+GTP)	22	20, 24	
V_{max} (+ATP)	4.3	3.7, 4.9	5
$K_{ic(ATP)}$	1500	1100, 1900	
$K_{iu(ATP)}$	1900	1200, 2500	

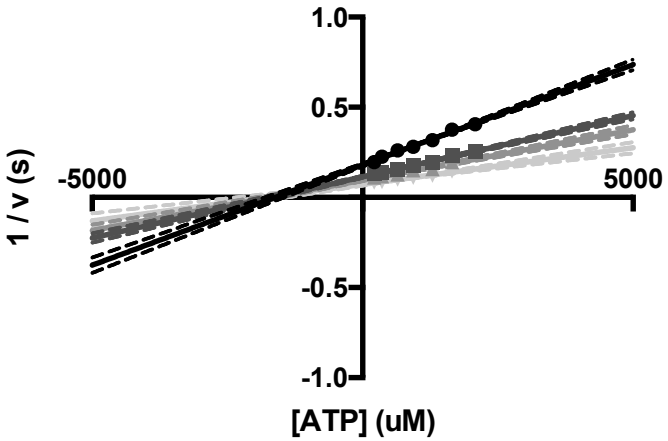

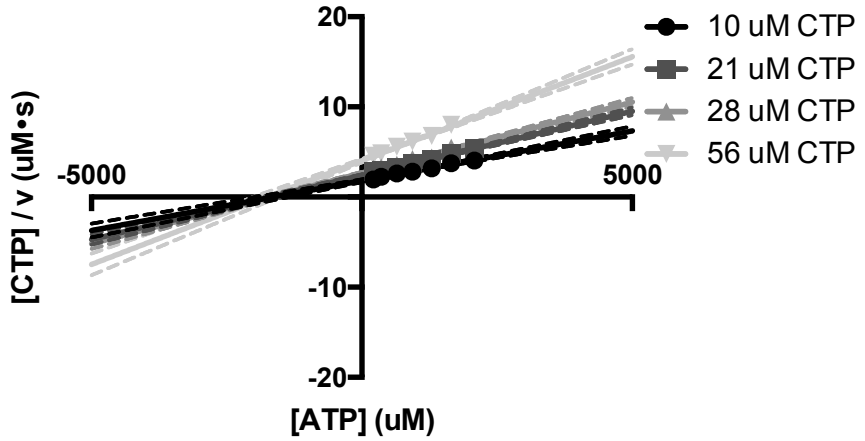

FIG 2.4 ATP is a mixed inhibitor of CTP incorporation. *Upper left*: Michaelis-Menten plots of CTP incorporation in the presence and absence of inhibitors. *Lower panel*: Dixon (*left*) and Cornish-Bowden (*right*) plots of ATP titrations against four CTP concentrations. Dashed lines represent 95% confidence intervals from fitting the intersection. *Upper right*: Numeric values of kinetic parameters from graphical analysis. Calculated values of V_{max} and $K_{d(CTP)}$ at 4900 uM ATP are derived from $K_{ic(ATP)}$ and $K_{iu(ATP)}$.

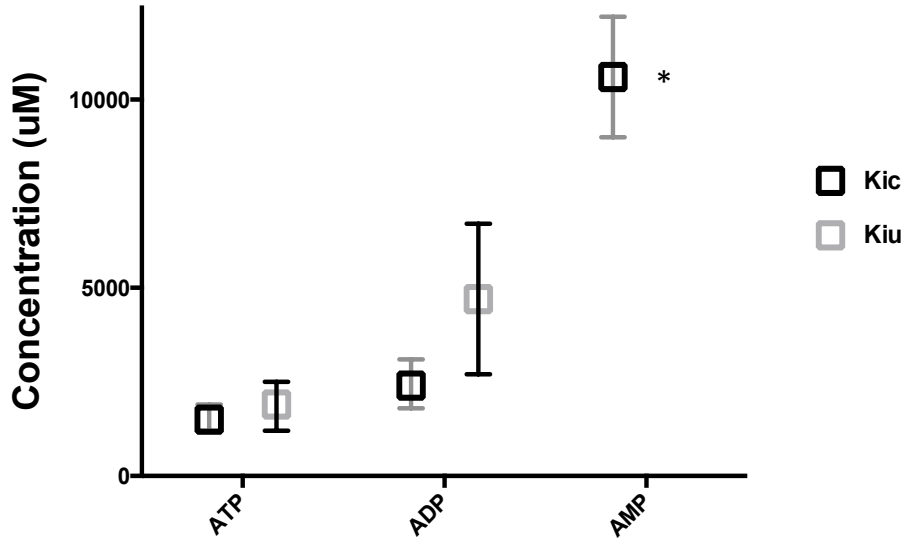

Substrate	K_{ic} (uM)	95% Confidence Limits Lower, Upper	K_{iu} (uM)	95% Confidence Limits Lower, Upper
ATP	1500	1100, 1900	1900	1200, 2500
ADP	2400	1800, 3100	4700	2700, 6700
AMP	10600	7300, 13900	N/A	

FIG 2.5 Phosphate requirements of ATP inhibition. Results of Dixon/Cornish-Bowden analysis of adenylate inhibition of CVB3 $3D^{pol}$. For AMP, there was not a well constrained fit for an intersection on the Cornish-Bowden plot, which is indicated by * in the graph and N/A in the table.

$K_{ic(GTP)}$ (data not shown), but both had an almost two-fold reduction in $K_{ic(ATP)}$ and a significant increase in $K_{iu(ATP)}$ (Figure 2.6). This indicates that ATP uncompetitive inhibition was weakened or even abolished (in the case of I230F) in these mutants, while competitive inhibition by GTP was unaffected and $K_{iu(ATP)}$ was reduced almost two-fold.

Since the side chains of I230 and F232 form part of a crevice that was identified as a candidate for being a ligand binding pocket (see Section 3.4.2), it was hypothesized that the allosteric site for ATP binding involved motif A and the effect of these mutations was to perturb ATP binding directly. A close analysis of the putative binding pocket shows that it is largely composed of peptide backbone and is therefore difficult to mutate (Figure 2.7). Surface-exposed histidine 228 forms the outer boundary of the pocket and due to its minimal interactions with other residues seemed a good candidate for mutagenesis that would perturb ligand binding without dramatic effects on local packing. Two mutant polymerases, H228A and H228E, were made and found to be active. Neither had a well-defined $K_{iu(ATP)}$, but both had $K_{ic(ATP)}$ values comparable to that of wild type $3D^{pol}$ (Figure 2.6).

To further assess the importance of this pocket in ATP binding, a less direct mutation, M310W, was made beneath the surface of the pocket (Figure 2.7). A tryptophan in this position would not directly alter the geometry of the pocket, but could cause local rearrangements that would likely interfere with ATP binding. A stable and active M310W polymerase was purified and used in elongation assays. The mutation was found to attenuate ATP uncompetitive inhibition about 50%, with milder effects on $K_{ic(GTP)}$ and $K_{ic(ATP)}$ (Figure 2.6).

Another proximal residue, phenylalanine 364, whose peptide backbone forms part of the rim of the putative binding pocket, has been found to be an important residue for fidelity (McDonald *et al.*, submitted). An F364W mutant strain was found to be stable *in vivo* with an

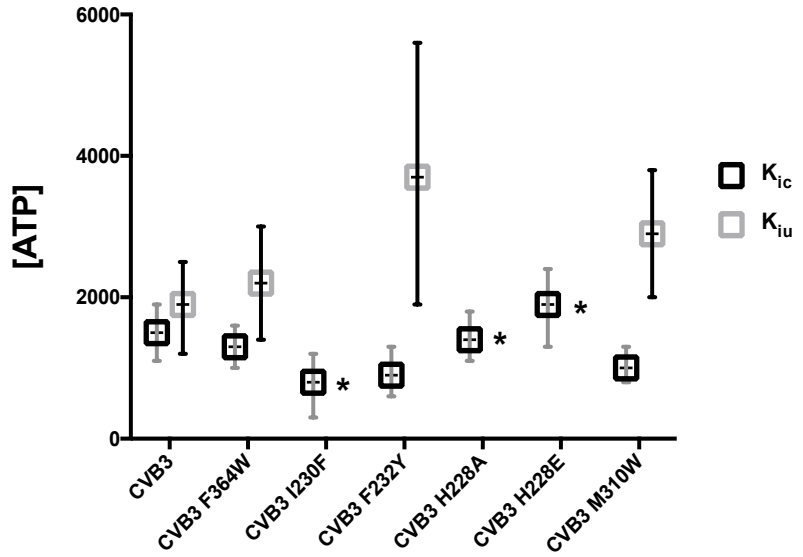

CVB3 Mutant	$K_{ic(ATP)}$ (uM)	95% Confidence Limits Lower, Upper	$K_{iu(ATP)}$ (uM)	95% Confidence Limits Lower, Upper
Wild Type	1500	1100, 1900	1900	1200, 2500
F364W	1300	1000, 1600	2200	1400, 3000
I230F	800	300, 1200	N/A	
F232Y	900	600, 1300	3700	1900, 5600
H228A	1400	1100, 1800	N/A	
H228E	1900	1300, 2400	N/A	
M310W	1000	800, 1300	2900	2000, 3800

FIG 2.6 CVB3 mutant effects on ATP inhibition. ATP inhibition against six CVB3 mutants was evaluated by Dixon/Cornish-Bowden analysis. For I230F, H228A, and H228E, there was not a well constrained fit for an intersection on the Cornish-Bowden plot, which is indicated by * in the graph and N/A in the table.

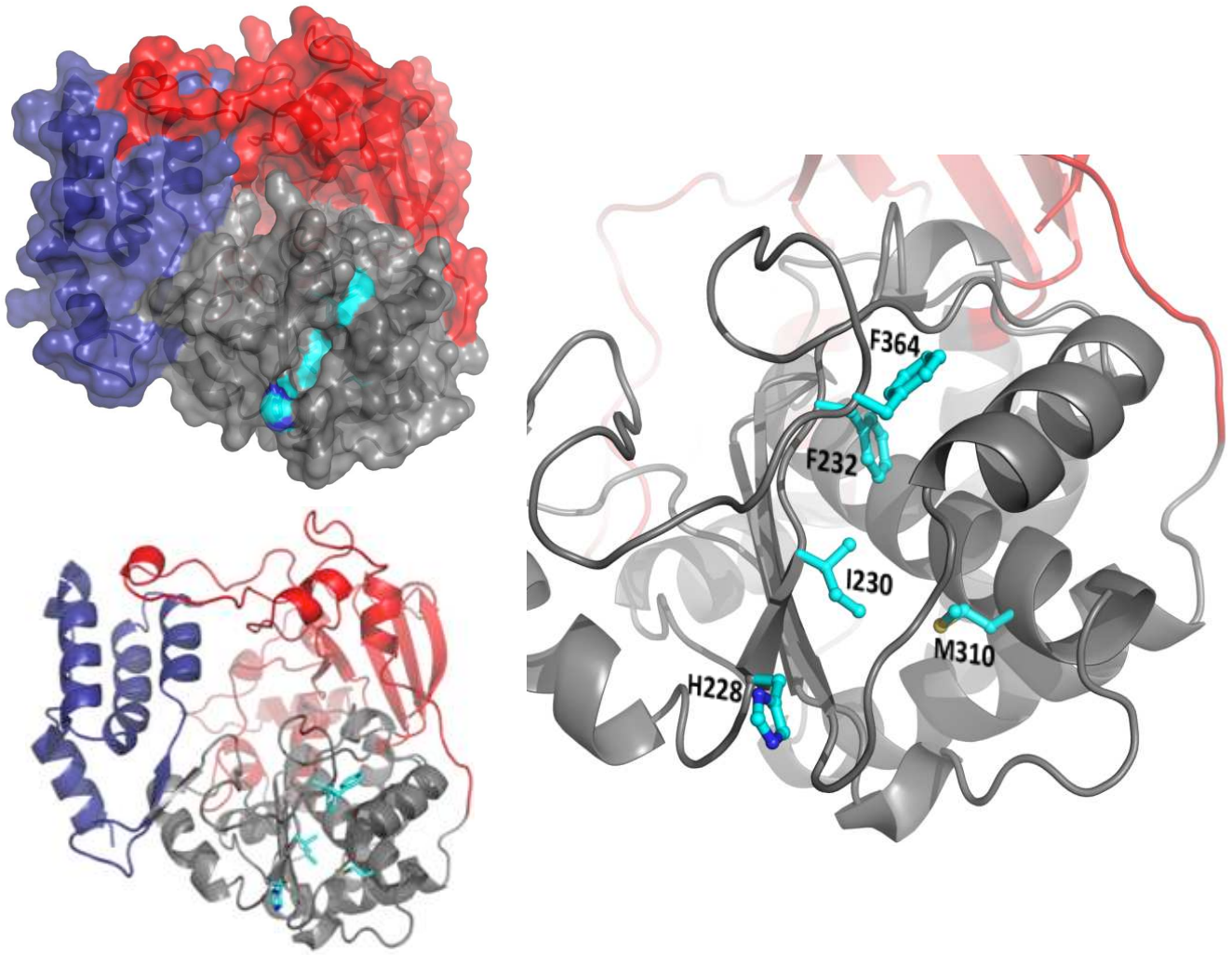

FIG 2.7 Mutated residues in CVB3 3D^{pol}. The polymerase is colored according to domains (red=fingers, grey=palm, blue=thumb). Residues that were mutated are colored according to atom type (cyan=carbon, blue=nitrogen, yellow=sulfur). *Upper left*: Surface representation of 3D^{pol} highlighting the position and depth of the pocket formed in part by the residues that were mutated. *Lower left*: Cartoon representation of the structure above with ball-and-stick representations of the side chains of the five residues of interest. *Right*: Close-up view of the mutated region.

increased replication fidelity phenotype. When used in inhibition assays, this mutant did not deviate significantly from wild type in any of the kinetic parameters (Figure 2.6).

2.3.5 The Mode of ATP Inhibition Varies across Picornaviral Species

From what is currently known of $3D^{pol}$ diversity among picornaviruses, coxsackievirus and poliovirus are at opposite poles of the speed and fidelity spectrum, with poliovirus polymerase being the fastest and most error-prone.[22] Since the above motif A mutants lowered CVB3 $3D^{pol}$ fidelity and increased its speed, pushing it toward the polio end of the spectrum, and also had a greatly reduced uncompetitive component of ATP inhibition, we hypothesized that ATP would have less of an effect on poliovirus polymerase. Indeed, Sabin strain OPV2 $3D^{pol}$ was found to have $K_{ic(GTP)}$ and $K_{ic(ATP)}$ values comparable to CVB3, but a $K_{iu(ATP)}$ could not be fit, indicating there is no significant uncompetitive component of ATP inhibition on this polymerase (Figure 2.8).

To determine how general mixed ATP inhibition is within *Picornaviridae*, four additional species were tested: two coxsackie type A species, CVA6 and CVA16, enterovirus 71 (EV71), and human rhinovirus C (HRVC). All four species had comparable competitive inhibition constants for GTP, though their $K_{ic(ATP)}$ values varied modestly (Figure 2.8). Other than HRVC, however, there was not clear indication of uncompetitive inhibition for any of these polymerases. In this regard, these species are more similar to poliovirus, with HRVC being intermediate. It would seem that the uncompetitive inhibitory effect of ATP on elongation is mostly specific to CVB3.

2.3.6 Kinetic Modeling

In order to corroborate the graphical analysis, kinetic simulation was performed using the computer program *Global Kinetic Explorer* (KinTek).[50,51] KinTek uses a discrete differential

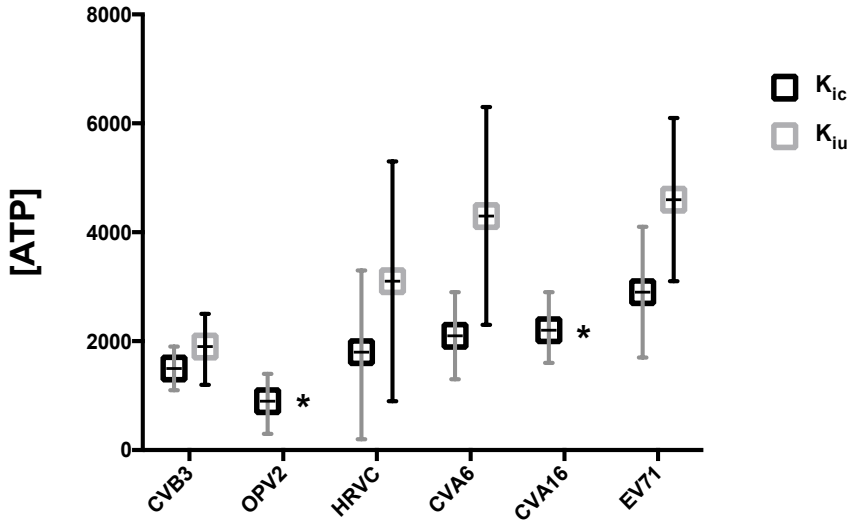

Polymerase Species	$K_{ic(ATP)}$ (uM)	Lower, Upper Confidence Limit	$K_{iu(ATP)}$ (uM)	Lower, Upper 95% Confidence Limit
CVB3	1500	1100, 1900	1900	1200, 2500
OPV2	900	300, 1400	N/A	
HRVC	1800	200, 3300	3100	900, 5300
CVA6	2100	1300, 2900	4300	2300, 6300
CVA16	2200	1600, 2900	N/A	
EV71	2900	1700, 4100	4600	3100, 6100

FIG 2.8 Mode of ATP inhibition across picornavirus species. ATP inhibition against six species of $3D^{pol}$ was evaluated by Dixon/Cornish-Bowden analysis. For OPV2 and CVA16, there was not a well constrained fit for an intersection on the Cornish-Bowden plot, which is indicated by * in the graph and N/A in the table.

equation solver to fit a user-defined model to experimental data. Once fed a dataset or multiple datasets along with initial conditions and information about which chemical species are observable, KinTek fits rate and non-rate parameters to the given model by minimizing χ^2. A major advantage of KinTek is that it can handle very complicated models and give rigorous error estimates of fitted parameters. The user defines which parameters are fixed and which can vary. Very conveniently, ratios of parameters can also be fixed, allowing for equilibrium constants to be inputted even without knowledge of the on- and off-rates.

The overall model that was input to fit stopped-flow datasets is schematized in Figure 2.2. The center species, ER4, represents the enzyme-RNA complex that has stalled after four incorporations because of the absence of CTP (see Figure 2.1). At this point, all four NTPs compete for the active site, CTP-binding alone being the productive pathway. All NTP on-rates were assumed to be equivalent while their off-rates were allowed to vary. Both before and after CTP binding, ATP can bind uncompetitively to the allosteric site, resulting in a singly liganded ER4A or a doubly liganded ER4CA complex that has a reduced rate of CTP incorporation. Catalysis results in an intermediate (ER5*) that then relaxes to another stalled complex (ER5). Both catalysis and relaxation are assumed irreversible on the time-scale of these experiments ($\leq$ 10 seconds).

The first experiment submitted for fitting was an eight-point titration of CTP from 12 to 120 μM with no inhibitors present. By global fitting of the model to all eight datatraces, V_{max} and $K_{d(CTP)}$ were determined and were in good agreement with values from the previous graphical analysis (Figure 2.9). These values were then fixed for the rest of the experiments. In the second experiment, a GTP titration from 200 to 2000 uM against 10 μM CTP was globally fitted to obtain a $K_{ic(GTP)}$ of 540 ± 80 uM, which was also within error of the value obtained from the

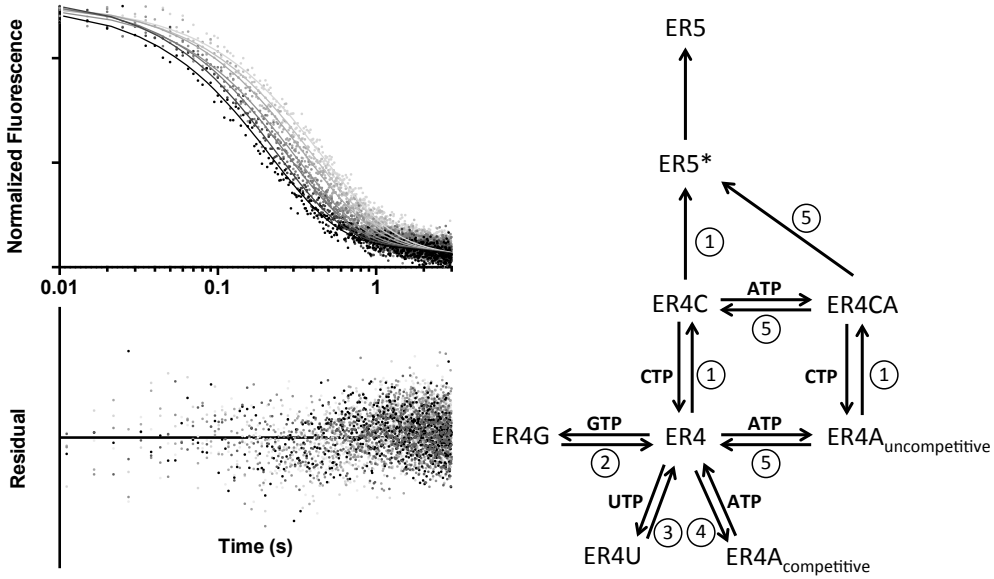

Experiment	Titrant	Constant	Graphical (uM)	KinTek (uM)
1	CTP	K_d	27 ± 6	24 ± 9
1	CTP	V_{max}	22 ± 1	20 ± 2
2	GTP	K_{ic}	440 ± 60	590 ± 80
3	UTP	K_{ic}	2900 ± 300	3100 ± 800
4	ATP	K_{ic}	1500 ± 200	1100 ± 200
5	ATP	K_{iu}	1900 ± 300	1800 ± 100

FIG 2.9 Kinetic modeling reproduces parameter values from graphical analysis. (*Upper left*) A representative KinTek fit of an ATP titration on a log timescale, with the residual plot below. (*Upper right*) The model from Figure 2.2 showing which experiment yielded the given parameter by numbering the equilibria according to the table below. The table lists the results from Michaelis-Menten and Dixon/Cornish-Bowden analyses alongside the values from the KinTek model (± standard deviation).

Dixon plot. Third, a UTP titration from 200 to 2000 μM also yielded a value in good agreement with the Dixon analysis, albeit with a large error since the titration was well below $K_{ic(UTP)}$.

Fitting $K_{ic(ATP)}$ and $K_{iu(ATP)}$ required two different experiments and additional assumptions. It was assumed that ATP- and CTP-binding did not affect each other; the only effect of uncompetitive ATP binding was to produce ER4CA, which had a reduced rate for CTP incorporation as compared to the uninhibited ER4C species. An ATP titration against constant CTP had a well-constrained $K_{ic(ATP)}$ but a poorly constrained $K_{iu(ATP)}$, whereas a CTP titration against a high concentration of ATP was just the reverse. So in the fourth experiment, $K_{ic(ATP)}$ was determined first by a titration of ATP from 200 to 2000 μM against 10 uM CTP without any uncompetitive pathway. This value was then fixed, and in the fifth experiment $K_{iu(ATP)}$ was determined by fitting a CTP titration from 50 to 500 μM against 4.8 mM ATP. Neither inhibition constant was appreciably different from the graphical analysis results. The rate of ER4CA going to ER5* was 5.5 ± 0.2, a roughly 4-fold reduction in catalytic rate.

A major advantage of kinetic simulation, especially the dynamic simulation KinTek uses in which the model instantaneously updates as parameters are varied, is the ability to judge which parameters are well constrained by the data.[46,50] For example, if two parameters are highly covariant and poorly constrained, i.e. one can compensate for the other, their confidence intervals fail to converge and large changes in their values have little effect on the overall goodness of fit by visual inspection or χ^2 analysis. This provides useful information about redundancy in the model and also serves as a test of how well the molecular events in the experimental system are understood. Even minor (≤ 2-fold) changes of the fitted values for the parameters described here caused the model to obviously deviate from the data. Additionally, no

two parameters had equivalent effects on the model, nor could the model compensate if any were omitted, which suggests that the mechanism was not over-parameterized.

2.4 Discussion

2.4.1 Competitive Inhibition

Unlike other classes of single-subunit polymerases, which use swinging motions in the fingers domain to move the incoming nucleotide and templating base into the active site after they have paired, RdRps have a fully prepositioned templating base in the active site, thereby coupling nucleotide discrimination with active site closure.[20] This implies that, in the cellular context, all four nucleotides are in direct competition for the active site and that fidelity depends greatly upon the polymerase's sensitivity to the geometry of the nucleotide. This sensitivity has been shown to be largely mediated by motions of motif A in response to a hydrogen-bond network between the palm domain and the ribose hydroxyl groups. As might therefore be expected, motif A mutants that lower fidelity also have a reduced ability to discriminate between CTP and 2'-deoxyCTP, though they do not significantly alter the affinity for CTP. This raised the question of whether these mutants only altered the dynamics of active site closure or also increased the affinity of the polymerase for non-cognate nucleotides. The inhibition experiments described here provide a tractable way to directly investigate the effects of fidelity mutants on this affinity.

The competitive inhibition constants for GTP and ATP roughly scale with their physiological concentrations for all species investigated, whereas $K_{ic(UTP)}$ in CVB3 $3D^{pol}$ is tenfold higher than its estimated cellular concentration. This is surprising since the templating base in this system is guanidine, with which uridine can base-pair better than the purines. One possible explanation for this may be the stronger pi-stacking interactions the purines can form

with the priming guanidine.[52] An alternative explanation could be that to compensate for a faster k_{cat} of UMP misincorporation, the polymerase has evolved a way to lower its affinity for UTP. Without determining k_{cat}, however, this remains speculation. It is interesting that the purine K_{ic} values are near their physiological concentrations, as this indicates that in the cell the polymerase could have significantly slower kinetics than what is suggested by studies in which only the cognate nucleotide is present. It also suggests that non-cognate nucleotides are by no means excluded from the active site, but rather occupy an appreciable portion of active sites at any given time.

The initial hypothesis that fidelity mutants may alter polymerase affinities for non-cognate nucleotides has been largely negated. $K_{ic(GTP)}$ hovers around 400 uM for all CVB3 mutants and also for the other species investigated, including poliovirus, which is known to have much lower fidelity than CVB3. $K_{ic(ATP)}$ varied more significantly among the polymerases, with almost 2-fold decreases in CVB3 I230F and F232Y as well as in poliovirus. However, as discussed below, $K_{ic(ATP)}$ values in CVB3 may be influenced by the uncompetitive component of ATP inhibition, making it more difficult to say whether the actual affinity of the active site for ATP is altered by these mutations.

2.4.2 Mechanism of ATP Inhibition

The Dixon and Cornish-Bowden analysis unambiguously identifies ATP as a mixed inhibitor of CVB3 $3D^{pol}$. An interesting consequence of the uncompetitive component of its inhibition is that ATP must bind an allosteric site on the enzyme. Allosteric regulation of nucleic acid polymerases by NTPs is not without precedent. Transcription initiation by *E. coli* RNA polymerase at a T7 A1 promoters has been shown to be allosterically inhibited by UTP.[53] ATP was also found to be a mixed inhibitor of HIV-1 reverse transcriptase elongation.[54] The hepatitis

C RdRp, NS5B, is stimulated by high concentrations of GTP.[55] GTP bound at a low affinity site on the surface has been observed in a crystal structure of NS5B.[56] Though mutational analysis indicates the GTP binding site in the crystal structure is not responsible for the observed stimulation *in vitro*, the site is important for replication *in vivo*.[57] Additionally, several allosteric inhibitors of NS5B bind near the GTP binding site.[58]

Beyond the implication of allostery, the data give other hints at the mechanism of ATP inhibition. The relatively small difference between $K_{ic(ATP)}$ and $K_{iu(ATP)}$ (400 uM) means that their effects on $K_{d(CTP)}^{app}$ should roughly cancel per the mixed inhibition equation $K_d^{app} = K_d\ (1 + [I]/K_{ic}\ )/(1 + [I]/K_{iu})$, but the Michaelis-Menten analysis shows a much larger than predicted effect (Figure 2.4). This may result from the fact that unlike classic mixed inhibition, in which the inhibitor is thought to bind only one site and produce a catalytically incompetent species, ATP is bound both in the active site and in an allosteric site. Not only so, we hypothesize that the allosterically bound ATP may not produce a catalytically inactive species but, rather, a species that has a reduced rate of CTP incorporation, especially since incorporating such a rate was required for the kinetic simulation. In this case, K_{ic} and K_{iu} as determined by graphical analysis do not represent true binding constants since the events which they dictate are not "dead ends" but rather have flux across them (i.e. from $ER4A_{uncompetitive}$ and ER4C to ER4CA to ER5) and are therefore not at equilibrium.[43] This may explain why in the I230F and F232Y mutants, in which uncompetitive inhibition was eliminated, the K_{ic} value decreased, which might reveal the "true" K_{ic} value for ATP competing for the active site and reconcile the Michaelis-Menten analysis with the Dixon/Cornish-Bowden result.

This mechanism is akin to hyperbolic inhibition, so named because the enzymatic rate approaches a non-zero value as inhibitor concentration goes to infinity due to an active enzyme-

inhibitor-substrate complex, causing the single reciprocal plot to look hyperbolic instead of linear at high inhibitor concentrations.[43] Though such curvature is not present in the Dixon and Cornish-Bowden plots, because of practical considerations (such as solubility, cost, Mg^{2+} concentration and ion effects, and a desire to stay within physiologically relevant concentrations), the concentration of ATP was only taken as high as ~2 mM, resulting in a predicted saturation of ~50%, which may be too low to manifest a hyperbolic tendency.

2.4.3 Significance

Regardless of the precise mechanism of ATP inhibition, its mixed profile is important for two reasons. First, the presence of an allosteric site, especially one that is amenable to biochemical assays by virtue of its effect on *in vitro* elongation, has important implications for drug discovery, as evidenced by the inhibitors that bind the GTP allosteric site on NS5B. This will be the subject of further investigation and discussion in Chapter 3.

Second, a regulatory relationship between $3D^{pol}$ and ATP has implications for polymerase function and host-virus interactions. The fact that ATP slows the polymerase is interesting in light of the fact that speed and fidelity are negatively correlated in $3D^{pol}$.[22] This may imply that ATP maintains viral RNA replication in a higher fidelity state. This is supported by the observation that ATP uncompetitive inhibition is abolished in the two low-fidelity, high-speed motif A mutants, I230F and F232Y, whereas it is at wild-type levels in the high fidelity motif D mutant, F364W.

In an attempt to measure ATP effects on fidelity, 2'-deoxyCTP discrimination assays were performed in the presence and absence of ATP (data not shown). Unfortunately and for unknown reasons, the experiments failed to yield consistent effects on K_d^{app} values, but the observed reductions in k_{pol} were consistently proportional for both CTP and dCTP incorporation.

This argues that ATP inhibition does not contribute to 2' OH based nucleotide discrimination, though due to the complex nature of ATP inhibition, the ratio of efficiency constants from this discrimination assay may not be a good measure of fidelity. Additionally, *in vivo* mutation rates of motif D mutants are not as well correlated with *in vitro* discrimination constants as they are for motif A mutants (McDonald *et al.*, submitted). The putative binding pocket suggested by the mutagenesis studies (see Figure 2.7) is at the interface between motifs A and D, which may leave room for the possibility that ATP affects fidelity. To determine real mutation rates, *in vitro* replication of genome-sized fragments in the presence and absence of high ATP concentrations and subsequent sequencing analysis would be necessary.

A possible biological implication of these findings occurs to us based on the fact that, of the nucleotides, it is ATP that slows the polymerase. Such specificity may suggest that this interaction participates in a regulatory network that enables the virus to sense its host cell's metabolic state. Many picornaviruses, including CVB3, preferentially infect proliferating cells and are at much higher concentrations during the G_1/S phase of the cell cycle than in the G_2/M phase.[59] Uniquely, CVB infection of quiescent cells results in the virus entering a latent state until the cells become replicative, an odd behavior from a virus usually considered highly cytolytic. How it could benefit the virus for its polymerase to be slowed at its peak time of infection, when nucleotide pools are high, is difficult to predict. One hypothesis can be offered based on the quasispecies theory of viral replication; perhaps the virus remains in a high-fidelity mode for the majority of its replication to ensure propagation of the genome that has successfully infected a host. Then, as it approaches lysis and the cell sickens, it favors a faster and sloppier replication to produce a burst of mutants, allowing for a broader quasispecies distribution.

Whether or not this is an accurate model, it is interesting that this unique ATP behavior is present only in the highest fidelity picornavirus we studied, a virus that has low tolerance for mutation, as evidenced by the fact that CVB3 mutator strains are attenuated *in vivo*. This may implicate ATP as an important component in maintaining polymerase fidelity and thereby CVB3 virulence.

Chapter 3

Potential Allosteric Sites on $3D^{pol}$

3.1 Introduction

The advantages of allosteric inhibitors discussed in Chapter I and the finding discussed in Chapter II that several allosteric inhibitors of HCV NS5B exploit the GTP binding site, suggest that an ATP binding site on $3D^{pol}$ could have pharmacological importance. This prompted a three-pronged search for potential allosteric sites on $3D^{pol}$, especially in CVB3. First, a general search for potential sites using two computer algorithms was made in three picornavirus species. Then an attempt was made at docking ATP into the sites found on CVB3 $3D^{pol}$. Finally, co-crystallization experiments with ATP and $3D^{pol}$ resulted in five different structures with resolutions ranging from 2.6 to 1.7 Å. Unfortunately, none of these efforts led to unambiguous identification of the ATP allosteric site, though the results suggest potential pockets whose role in ATP inhibition could be characterized through mutagenesis.

3.2 Materials and Methods

3.2.1 In Silico *Search for Allosteric Pockets*

The first program, CASTp (Computed Atlas of Surface Topography of proteins),[60] was chosen because it had previously been validated in an RdRp system. Malet *et al.* confirmed that CASTp could identify three previously characterized allosteric sites on the HCV polymerase, NS5B, and then used it to find possible allosteric sites on other flaviviral RdRps.[18] In simplified terms, the CASTp algorithm strips the structure of heteroatoms and probes the surface and interior with a 1-10 Å sphere to identify surface pockets and interior voids. It then measures the

volume by both the solvent accessible surface model (Richards surface) and the molecular surface (Connolly surface).[61]

Another program, PARS (Protein Allosteric and Regulatory Sites), was used to validate the CASTp findings because it uses a different algorithm for identifying surface pockets.[62] Simply stated, PARS uses the LIGSITE algorithm[63] to map the protein onto a grid; any grid point within 3 Å of an atom coordinate is deemed to be protein and any grid point outside that radius is considered solvent. If enough solvent grid points are encompassed by protein, they are considered a pocket.[64] A dummy ligand is then modelled into each site and a normal mode analysis (NMA) dynamics calculation is performed on the apo and liganded structures. Finally, hits are ranked by significance of dynamic differences and structural conservation. NMA *p*-values of ≤ 0.05 and conservation scores of >50 are considered significant.

3.2.2 ATP Docking

ATP with deprotonated phosphates was subjected to quantum mechanical calculations to determine the partial charges on each atom. High level *ab initio* methods using second order Møller-Plesset (MP2) calculations were used to derive restrained electrostatic potential (RESP) charges, specifically using the 6-31G* basis set, which is most appropriate for an effective two-body model for simulations in polar media. The program Antechamber (part of AmberTools 13) was used to assign partial charges based on the *ab initio* calculations using the AMBER force field. The receptor, the elongation complex structure of CVB3 $3D^{pol}$ (PDB code: 4K4Y), was prepared for docking with Chimera structure editing tools, including assignment of Gasteiger charges and addition of hydrogens using AMBER. Docking experiments were performed using the Autodock Vina plugin in The PyMOL Molecular Graphics System, Version 1.8 (Schrödinger, LLC) implemented by the SBGrid Consortium.[65,66]

3.2.3 Crystallography

Purified CVB3 $3D^{pol}$ was concentrated to between 6 and 12 mg/mL, combined with a final concentration of 10 mM ATP, and crystallization trays with Qiagen JCSG+ and Cryos crystallization suites were set up using an Art Robbins Gryphon robot. Crystals were shipped to the Advance Light Source for synchrotron data collection on MBC beamline 4.2.2.

3.3 Results

3.3.1 Potential $3D^{pol}$ Allosteric Sites

Unfortunately, there is no published structure of an allosteric regulator of $3D^{pol}$ elongation in complex with the polymerase. Because of this, an *in silico* search for potential sites on the polymerase surface was conducted. Three well-studied picornaviral species with published $3D^{pol}$ structures were selected as representative structures: Poliovirus (PV), Coxsackievirus B3 (CVB3), and Enterovirus 71 (EV71).[ǂ1] All three structures are very homologous, but *in vitro* studies have shown vastly different speeds and fidelity at least for CVB3 and PV polymerases.[22] As an initial search, the following selection criteria were applied: sites must reside outside the active site cavity of the protein, be of (molecular surface) volume >100 $Å^3$ as calculated by CASTp, and also be identified by PARS. The results are shown in Figure 3.1.

Altogether, four potential sites met the selection criteria: (i) the exterior base of the thumb domain seen in all three polymerases (T-Site), (ii) a site between the fingers and palm domains seen in PV and EV71 (FP-Site), (iii) the interface between motifs A and D of the palm domain seen in CVB3 and EV71 (P-Site), and (iv) the point of contact between the fingers and thumb domains seen in EV71 (FT-Site). Additionally, the top of the fingers domain in the PV and EV71 polymerases had crevices that met the criteria, but were not considered here because they were

[ǂ] PDB codes in order: 1RA6, 3DDK, 3N6L.

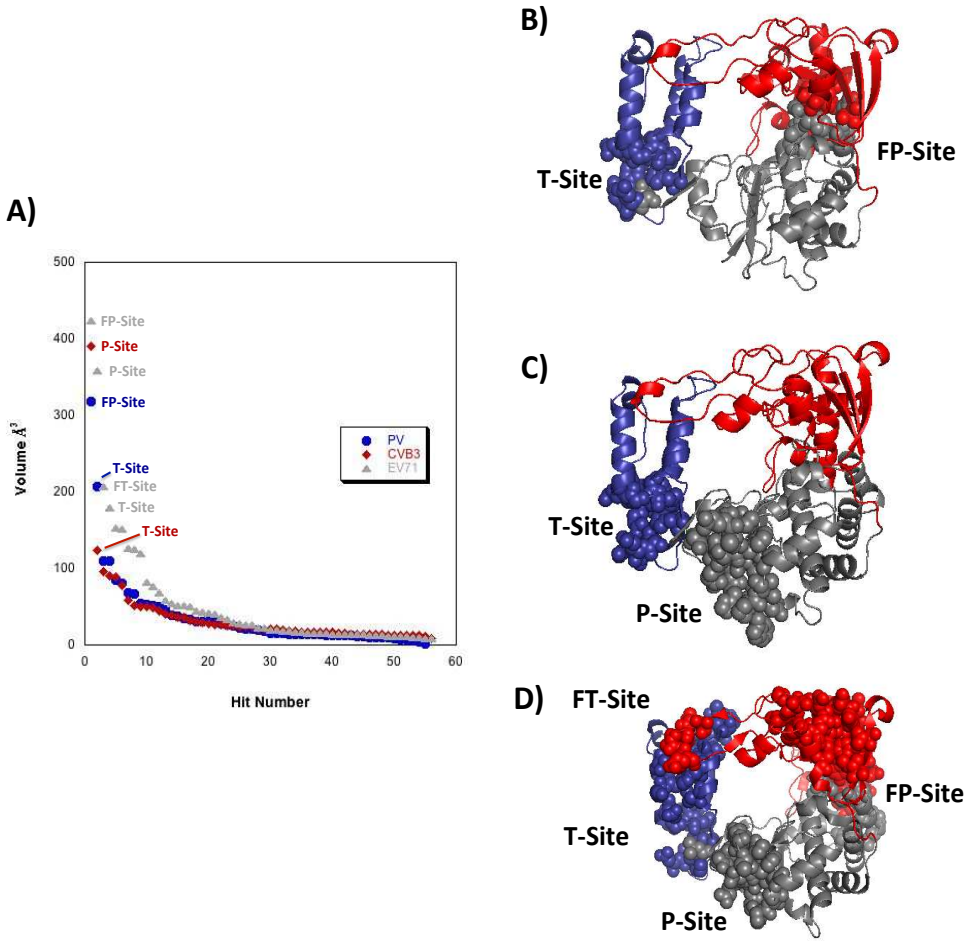

FIG 3.1 Potential allosteric sites on 3D^{pol} from three species. Polymerases are colored by major domains: fingers (red), palm (grey), and thumb (blue). The sites that met the selection criteria are shown as spheres. (A) Results of the CASTp search are plotted; outliers are labeled for each species. (B) PV 3D^{pol} has two sites.: (1) the N-terminal region of the thumb domain, and (2) the junction of the fingers and palm domains. (C) CVB3 has two sites: (1) the N-terminal region of the thumb domain, and (2) the interface of palm motifs A and D. (D) EV71 has the three sites found in the other polymerases and an additional site at the junction of the thumb and fingers domains.

intermediate between outliers and noise in the volume plot and because they were shallow crevices over large surface areas rather than well-defined pockets.

Interestingly, two of these sites seem to correspond with allosteric sites on the thumb domain of HCV NS5B (PDB code: 1C2P) that are known to bind nonnucleoside analogue polymerase inhibitors and GTP (Figure 3.2).[58,67] The $3D^{pol}$ T-Site and NS5B Thumb Site II bear some similarities (Figure 3.3 B & D). They both are at the N-terminus of the thumb domain where three alpha-helices come together to form a pocket undergirded by two anti-parallel beta-strands. The bottom of the pocket is formed by an aromatic residue (histidine in $3D^{pol}$, tyrosine in NS5B) surrounded by polar and charged residues. There is also resemblance between the $3D^{pol}$ FT-Site and the NS5B Thumb Site I (Figure 3.3 A & C), both of which reside between the extended loop of the fingers domain and the thumb domain. A similar pocket to the one just described occurs in both polymerases at this site, wherein an important histidine is on the underside of a mostly polar and charged crevice. Such similarities bode well for discovering allosteric regulators of $3D^{pol}$ based on the platform of well-established NS5B inhibitors.

The largest pocket on CVB3 polymerase and the second largest on EV71 were at the P-Site (Figure 3.1 A), which does not have a known counterpart in NS5B. In both polymerases, the pocket is at the "backside" of the polymerase just below the NTP entry channel, and is formed by the interaction between a motif D loop and a motif A loop within the palm domain (Figure 3.4). Interestingly, this pocket is largely comprised of the residues mutated in Chapter II. Similar to the pockets described above, this one also has a hydrophobic core composed of an aliphatic residue and a phenylalanine surrounded by polar elements mostly from the peptide backbone.

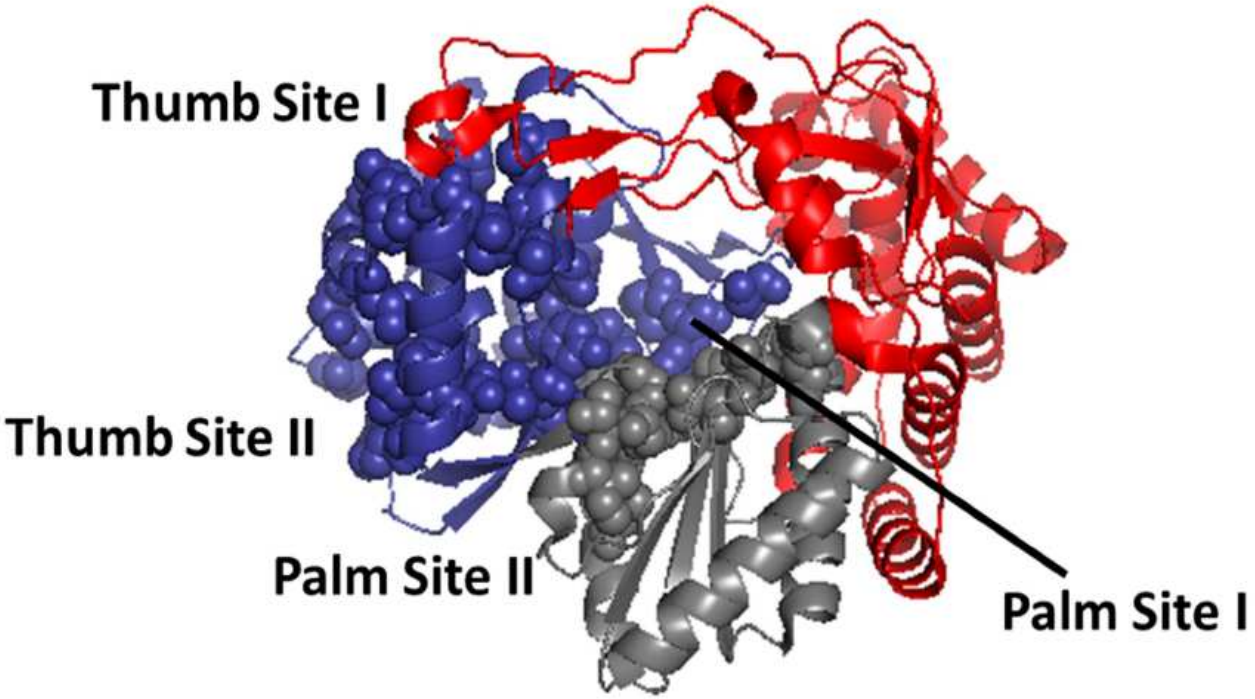

FIG 3.2 Allosteric sites on HCV NS5B. Polymerase is colored by domain as previously. Sites are indicated by spheres.

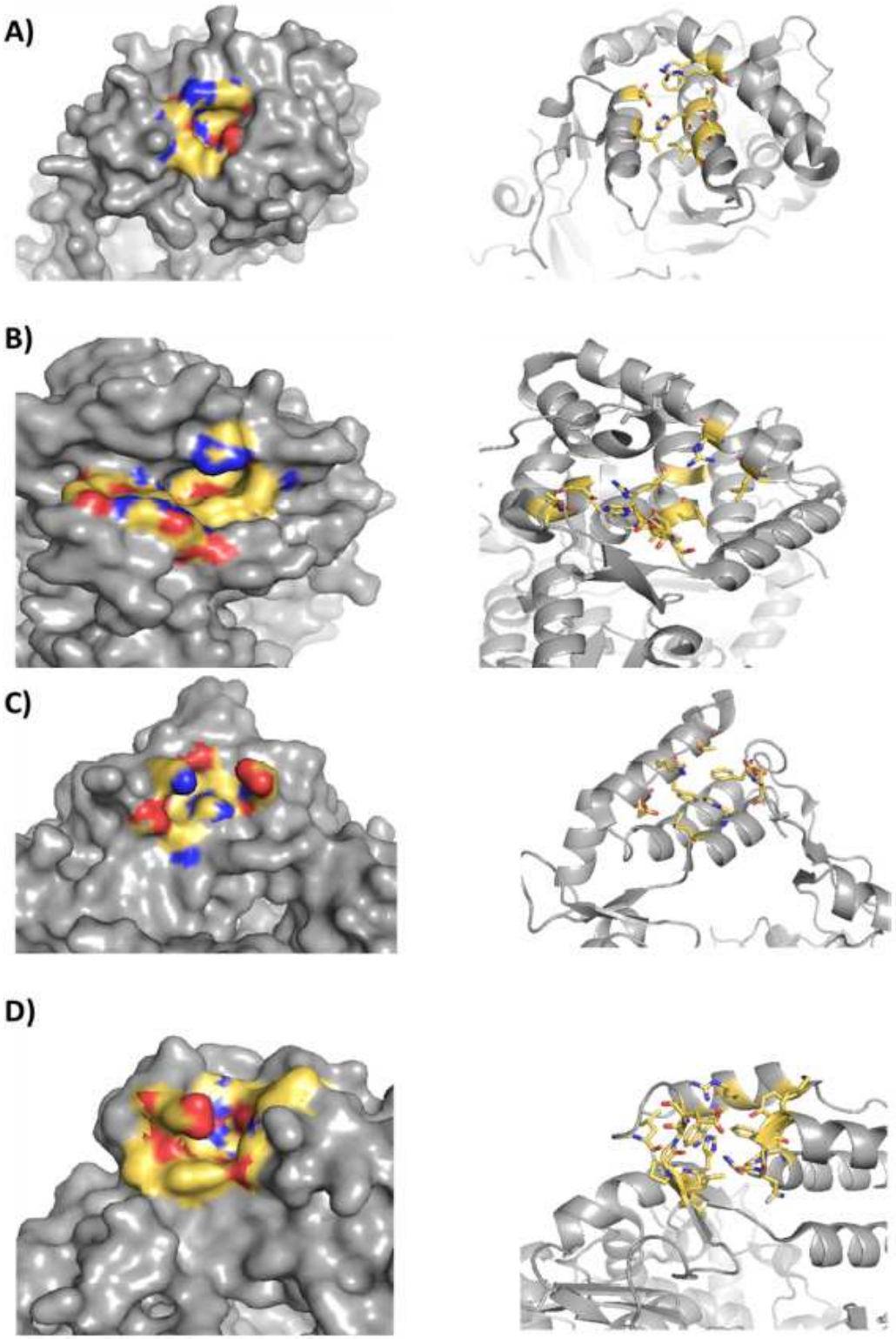

FIG 3.3 Comparison of binding sites on NS5B and 3D^{pol}. Surface representations of the pockets colored by atom type (C yellow, N blue, and O red) are paired with their stick representations (right). (A) Thumb Site I. (B) Thumb Site II. (C) TF-Site. (D) TP-Site.

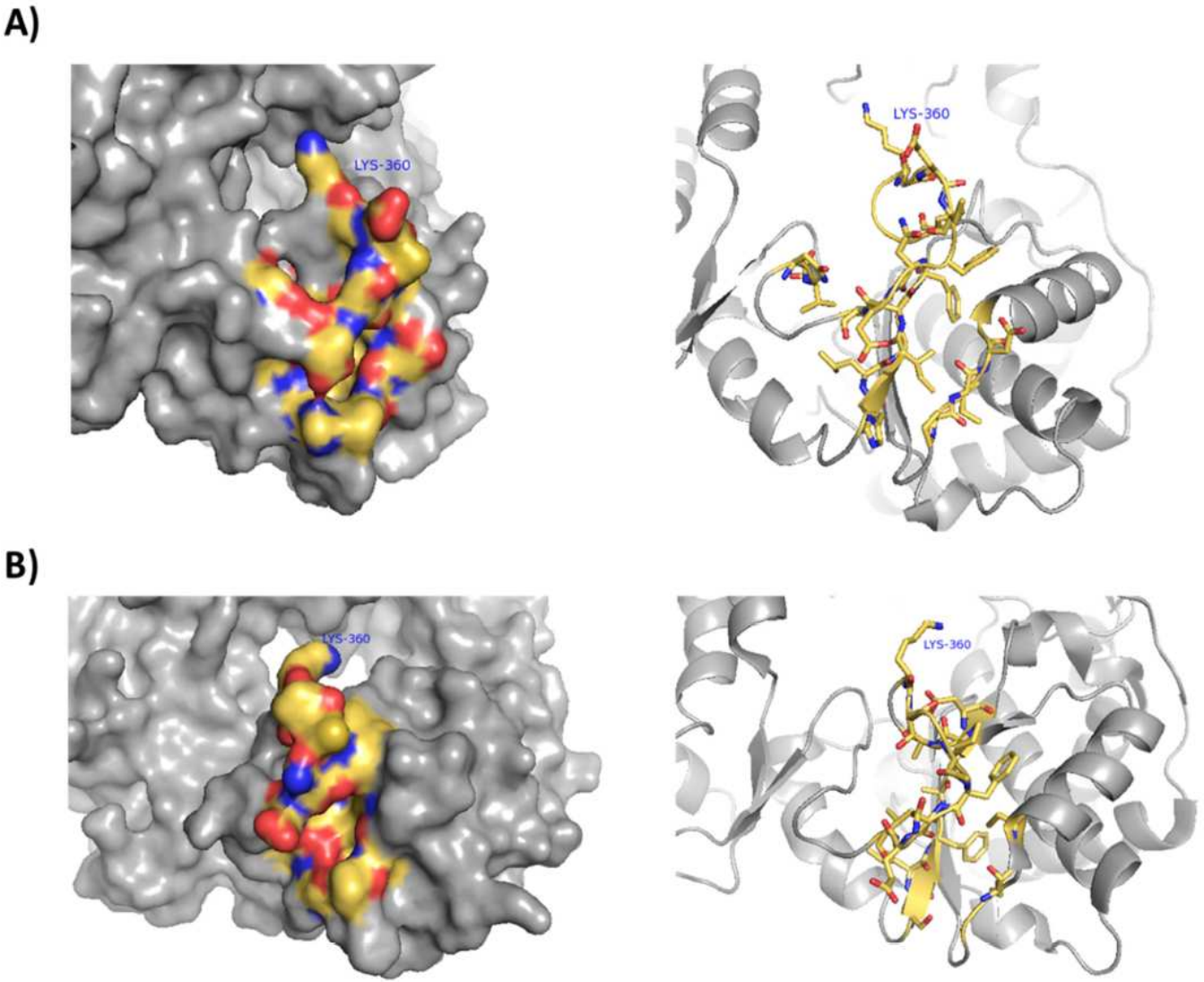

FIG 3.4 Comparison of P-Sites on CVB3 and EV71 3D^{pol}. Surface representations of the pockets colored by atom type (C yellow, N blue and O red) are paired with their stick representations (right). (A) CVB3. (B) EV71.

The largest pockets on both the EV71 and PV polymerases were at the FP-Site, where an alpha-helix of Motif B in the palm domain packs against the middle finger (Figure 3.5). Both pockets are deep and mostly hydrophobic, with a Ser288-Gly289-Cys290 sequence at the bottom of each. Entrance to this site in the PV structure is blocked by flanking tyrosines, greatly reducing the Richards surface but not the Connolly surface (data not shown).

3.3.2 ATP is Accommodated by the P-Site

The mutagenesis experiments in Chapter II and the *in silico* search above suggested the P-Site as a plausible site for ATP binding. Docking experiments were performed and several solutions showed ATP binding in the pocket. An example fit is pictured in Figure 3.6. However, among the dozens of docked positions, there was not a consensus orientation of the molecule in the pocket. In any given experiment, however, multiple and very different orientations were essentially isoenergetic, and from experiment to experiment the most favored orientations were not consistent, nor were they significant outliers in the output scoring function (data not shown). Also, as can be seen in Figure 3.6, there were not any atomic interactions that would obviously explain a strong preference for ATP over other nucleotides, since the docking was largely driven by polar contacts between the receptor and the phosphorylated ribose. Hence, it cannot be concluded from these experiments that this is the site of ATP binding. However, they do show that ATP can fit inside the pocket and establish a hydrogen-bonding network with the protein.

3.3.3 Electron Density for ATP was not Observed

As summarized in Table 3.1, five crystal structures of wild type CVB3 $3D^{pol}$ were solved with resolutions ranging from 2.6 to 1.7 Å, including one structure with a new space group for $3D^{pol}$. However, close analysis of the difference density maps showed no compelling

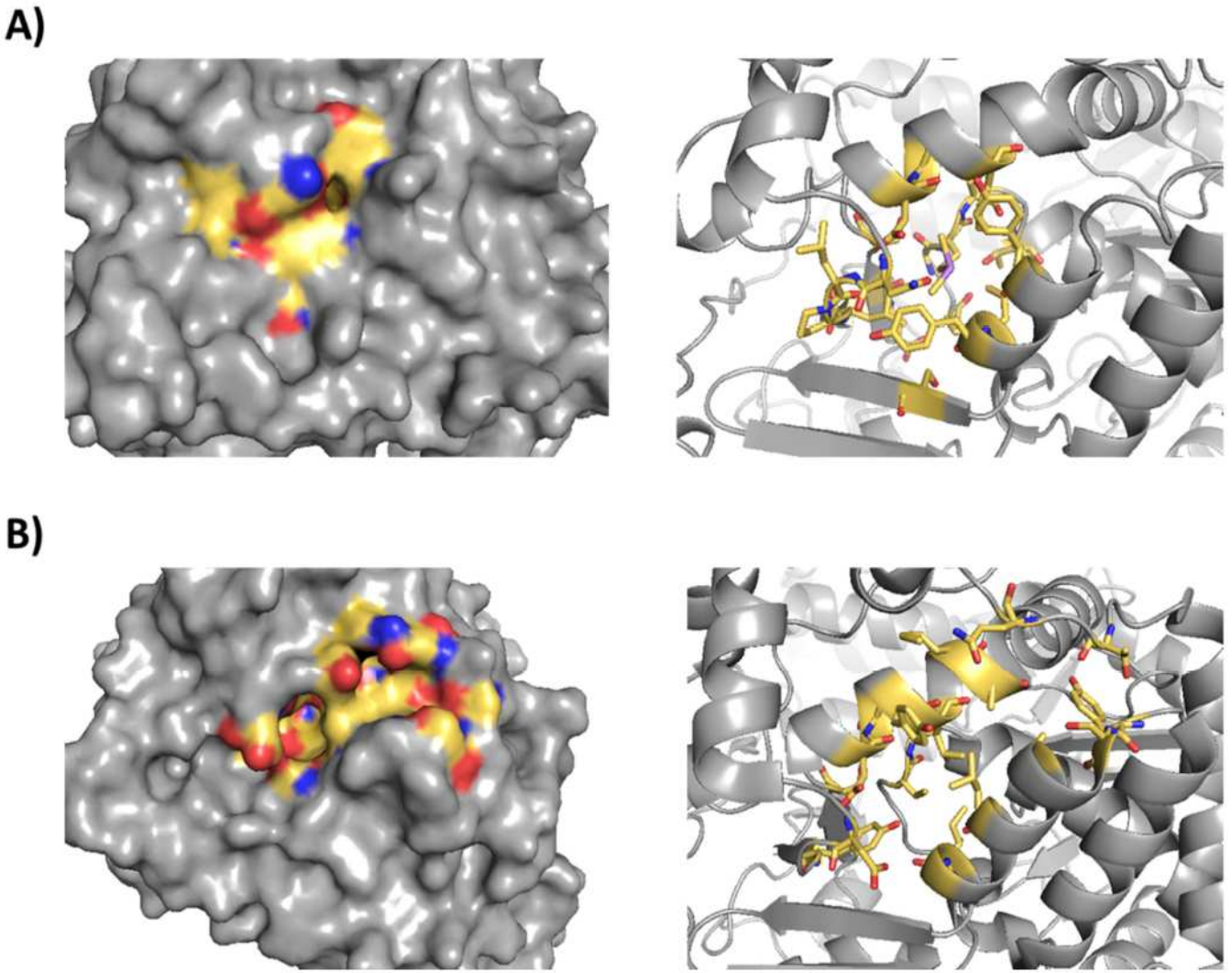

FIG 3.5 Comparison of FP-Sites on PV and EV71 3D^{pol}. Surface representations of the pockets colored by atom type (C yellow, N blue, and O red) are paired with their stick representations (right). (A) PV. (B) EV71.

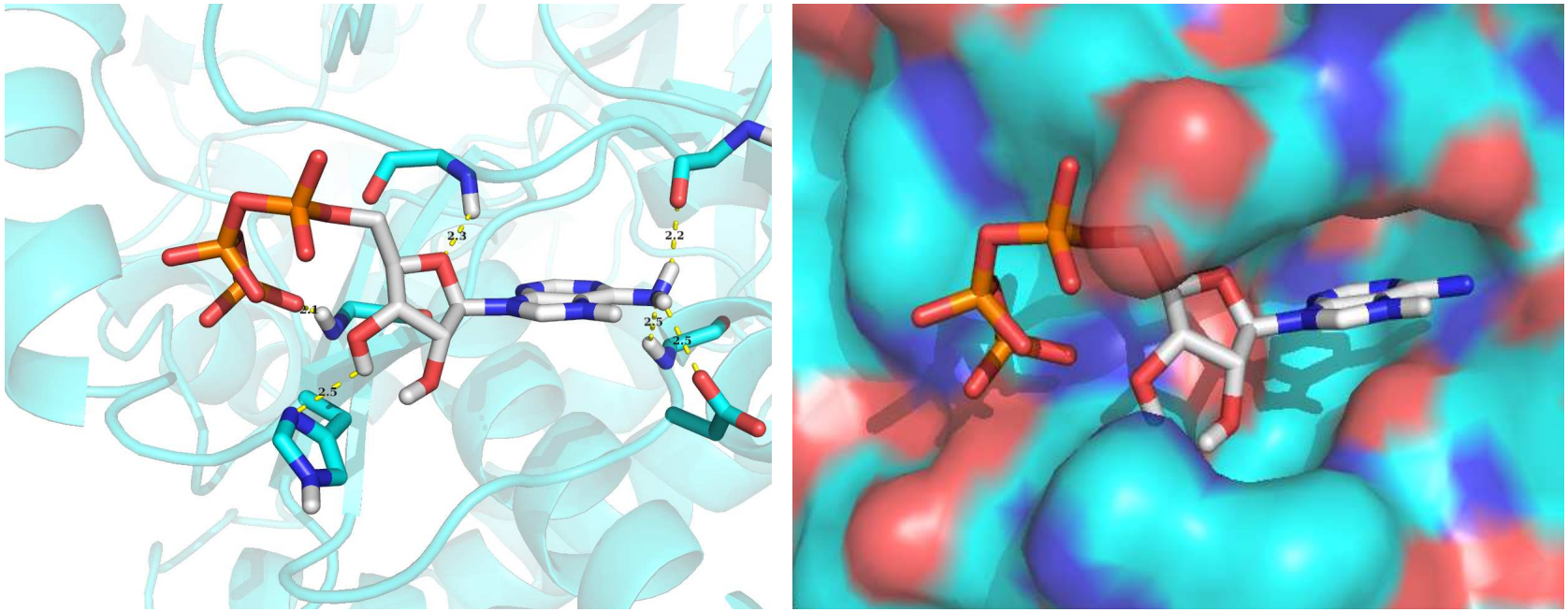

FIG 3.6 Putative binding pocket can accommodate an ATP. *Left*: A cartoon representation of the binding pocket with potential hydrogen bond partners and the docked ATP shown as sticks. Potential hydrogen bonds are indicated by measurements (yellow dashes). *Right*: The same docking solution with the receptor displayed as a solvent accessible surface. Note the depth of penetration of the adenine base into the largely hydrophobic pocket.

Table 3.1 Summary of CVB3 $3D^{pol}$ crystallization conditions and structures.

Crystal Number	Screen Conditions	Protein Drop:Mother Liquor Ratio	Space Group	Unit Cell Dimensions (Å)	Resolution (Å)
1	0.085 M sodium phosphate 0.085 potassium phosphate 0.085 M MES pH 6.5 1.7 M sodium chloride 15% glycerol	3:1	$P4_32_12$	75.75 x 75.75 x 292.8	2.5
2	0.085 M sodium phosphate 0.085 potassium phosphate 0.085 M MES pH 6.5 1.7 M sodium chloride 15% glycerol	1:1	$P4_32_12$	75.35 x 75.35 x 291.8	2.3
3	0.085 M HEPES pH 7.5 3.655 M sodium chloride 15% glycerol	1:1	$P4_32_12$	74.19 x 74.19 x 287.8	1.7
4	0.075 M HEPES pH 7.5 1.125 M lithium sulfate 25% glycerol	3:1	$P4_32_12$	74.48 x 74.48 x 290.0	2.6
5	0.075 M HEPES pH 7.5 1.125 M lithium sulfate 25% glycerol	1:1	$C222_1$	105.2 x 105.3 x 289.1	2.5

evidence for an ATP bound either in the putative palm domain binding pocket or anywhere else in the structures.

3.4 Discussion

3.4.1 The Importance of Allostery

There is an urgent need for antivirals to treat picornaviral diseases, which have historically been combated mainly with vaccines, if at all. Of the several potential pharmacological targets, the RNA polymerase $3D^{pol}$ is an attractive one because of its vital role in determining the kinetics of virus lifecycle and the genetic diversity of progeny virus, both of which are important factors for virulence and tropism. Additionally, $3D^{pol}$ performs chemistry not present in eukaryotic cells, RNA-templated RNA synthesis, which could allow for bioorthogonal disruption of its function.

There are two classes of drugs against viral polymerases that represent two main strategies of treatment. The first is to target the active site with nucleoside analogues that function as chain terminators or mutagenesis accelerators to push viruses off the cliff of error catastrophe. These molecules have met with success, ribavirin especially, but are problematic for several reasons, one of which is their nearly unavoidable tendency to produce off-target effects. The second strategy, which most often uses nonnucleoside analogues, is to target other sites of the polymerase to inhibit template binding, nucleotide binding, initiation, or elongation. Several reports have identified global dynamics and allosteric effects of the polymerase as important contributors to each of these crucial events. Hence, allosteric sites on the polymerase could be attractive targets of small molecule inhibitors.

Exploiting allostery has been extensively used in designing inhibitors of HCV NS5B, and has produced several drugs that have reached clinical trials.[68,69] The mechanisms of action of this

class of inhibitors are not fully known, though proposals based on crystallographic structures of polymerase-inhibitor complexes have been made. Generally, they are thought to work by limiting polymerase dynamics and/or preventing association with RNA and other proteins via inducing conformational changes. It is known that Thumb Site I inhibitors only affect initiation, not processive elongation.[58] There is also evidence that Thumb Site II inhibitors work by restricting the motions of a structural motif in the active site.[70]

So far, however, there is an unfortunate dearth of such sites identified on picornaviral RdRps. There is also a general shortage of drug screens reported against $3D^{pol}$. One was performed by the Peersen group and identified several nucleoside analogue leads, but no allosteric inhibitors were found.[71] The body of literature for natural allosteric sites on $3D^{pol}$ is also unfortunately small, almost all of it being concerned with a large protein-protein interface that is not vital for polymerase activity or the virus.

3.4.2 Potential Sites Identified by Cavity Searches

To address this lack, a computational search was made with CASTp and validated by PARS using three important species of $3D^{pol}$. After application of selection criteria, the search resulted in four main sites present on the three polymerases to different degrees. Two sites in the thumb domain roughly correspond to Thumb Sites I and II on HCV NS5B. Two sites without NS5B-counterparts were also identified, one in the fingers domain and another in the palm. Both programs identified the active site of the protein, which serves as a positive control for their ability to find important cavities. The four sites, FP-Site, FT-Site, P-Site, and T-Site were sites of greatest volume and tended to have the highest PARS ranking after the active site. Other than the active site, PARS did not assign significance to any other site based on either NMA or conservation analysis, but neither did it assign NMA significance to the NS5B allosteric sites

which it otherwise correctly identified (data not shown). This is perhaps unsurprising given how simplified the dynamics simulation is and also how subtle motions of these polymerases are thought to be. There were also many sites at or beneath the volume threshold on the thumb and fingers domains, especially on EV71 $3D^{pol}$. Though these were ruled out in this initial search, they retain potential as allosteric sites. Last, it should be mentioned that what CASTp deemed the interior cavity site extended further out into the periphery of the PV structure than the other two, and so pockets that could be considered may not have been because the program grouped them with the interior.

It is promising that two of the sites have precedence in HCV NS5B. However, there are several caveats associated with these findings. First, the relationship between $3D^{pol}$ and NS5B is distant, even though they belong to the structurally conserved RdRp family. That there are sites on $3D^{pol}$ that correspond to those on NS5B does not necessarily imply similar functions or binding modes. This is especially true for comparisons between Thumb Site II and the T-Site, since Thumb Site II inhibitors are thought to work by constraining the movements of a beta-loop, which is not present in $3D^{pol}$, during a transition from initiation to elongation.[70] Second, despite the similarities between the $3D^{pol}$ and NS5B sites, even a brief glance at the surface representations of their structures shows that they have very different anatomy, with those on NS5B having greater volumes.

In addition to being the largest pocket on EV71 and PV polymerases, the FP-Site could serve an important function in polymerase activity that makes it attractive as a potential allosteric site. In their structural characterization of template translocation, Sholders and Peersen observed three distinct structural transitions of the abovementioned Ser288-Gly289-Cys290 sequence, which, in conjunction with biochemical data, led to a model in which the motif B loop mediates

translocation.[72] In the *in/up* conformation, the sidechains of both Ser288 and Cys290 are buried in a hydrophobic pocket directly underneath the FP-Site. As the polymerase transitions to the catalytically active state, the B-loop adopts an *in/down* conformation wherein Ser288 flips down to hydrogen bond with a Motif D aspartate. Post-catalysis, Cys290 also flips out of the pocket in the *out/down* conformation during pyrophosphate release and may mediate translocation by clashing with the RNA. Mutating each of these three residues interfered with or abolished different steps of the catalytic cycle. Moreover, Verdaguer and colleagues have suggested the B-loop as a prime target for allosteric regulation of $3D^{pol}$ since there is evidence of its allosteric regulation in the Birnavirus RdRp.[73] In Birnavirus, viral protein VP3 binds the RdRp and induces a transition in which the B-loop transitions from a closed to open conformation to allow for template binding. The authors also note that a drug that blocks the template channel of dengue virus RdRp has proven an effective inhibitor. Hence, if an allosteric regulator could bind the FP-Site and hamper the motions of motif B, it could significantly inhibit polymerase activity.

3.4.3 The P-Site Seems the Most Promising

Although the P-site does not correspond to either Palm Site I or II on NS5B, it is nevertheless interesting for several reasons. First, it has a hydrophobic platform in the form of an isoleucine surrounded by polar and charged residues (Figure 3.5), one of which is a histidine opposite a glutamate that together coordinate a sulfate and a sodium in some $3D^{pol}$ structures (not shown). A mostly hydrophobic pocket with a critical hydrogen bond partner is characteristic of most of the NS5B allosteric sites.[68] Second, the pocket is formed by motifs A (residues 230-241, CVB3 numbering) and D (360-366) just below the strictly conserved Lys360, which conspicuously protrudes into the active site and which is necessary as a general acid for catalysis.[21] It has also been shown that the swinging motions as well as the protonation of this

residue are required for active site closure, underscoring its indispensable and dynamic role.[27] This provides a plausible mechanistic link between ligand binding and effects on catalysis. Third, a vaccine-derived T262I mutation in PV resulted in a mutator phenotype,[24] and point mutations of CVB3 residues 230 and 232 in motif A that directly interact with motif D resulted in fast, low fidelity polymerases *in vitro* and mutator phenotypes *in vivo*.[22] Moreover, these mutations abolished uncompetitive inhibition by ATP, suggesting that they interfere either with the binding of ATP or with its mechanism of inhibition. This pocket is also by far the largest allosteric site on CV $3D^{pol}$ identified by CASTp and was shown by the docking experiments to be capable of binding an ATP molecule. Because of these observations, the H228A, H228E, and M310W mutations were designed and tested (see Figure 2.6). The H228 mutants abolished uncompetitive inhibition by ATP, and the M310W mutation increased $K_{iu(ATP)}$ by more than 2-fold, confirming that this area of the palm domain is a determinant of ATP inhibition. Interestingly, a phenylalanine to tryptophan mutation of the neighboring 364 residue, which has been identified by the Peersen group as an important regulator of fidelity, had no effect on ATP inhibition. This residue exists at the interface of motifs A and D, just above the 230 and 232 residues (i.e. directly above the putative pocket), though its side-chain points away from the pocket. The fact that mutating this residue significantly affects local dynamics but does not affect the structure of the proposed pocket and does not perturb ATP inhibition, suggests that the other mutants may have a more direct effect in blocking ATP binding.

However, extenuating pieces of evidence preclude asserting that this is the allosteric ATP binding pocket. First, it provides no obvious structural basis for the biochemically observed specificity for ATP over GTP. Indeed, docking experiments comparing adenine and guanidine showed a slight preference for guanidine due to its extracyclic oxygen that can participate in

additional hydrogen bonds (data not shown). An argument could be made that because GTP has one more extracyclic group it may not be able to fit into an adenine binding pocket; however, there was not a significant difference in the depths of penetration between guanidine and adenine in these experiments. Symptomatic of this lack of specificity is the broad distribution of ATP conformations bound in this site and the resulting absence of a consensus orientation for any part of the molecule. To be confident in assigning the allosteric site, a structure with ATP bound would be necessary. Unfortunately, we were unable to attain such a structure through crystallography, possibly due to the millimolar affinity suggested by $K_{iu(ATP)}$ being further weakened by the usually high salt screening conditions. However, NMR experiments that are sensitive to the dynamics of this area of the polymerase[26] may be capable of determining whether or not ATP binds this pocket. Perhaps a fluorotryptophan[74] at position 364 could provide a readout of such an interaction, if it exists.

References

1. Rotbart, H. A. Treatment of picornavirus infections. *Antiviral Res.* **53,** 83–98 (2002).

2. Whitton, J. L., Cornell, C. T. & Feuer, R. Host and virus determinants of picornavirus pathogenesis and tropism. *Nat. Rev. Microbiol.* **3,** 765–776 (2005).

3. Holland, B. Y. J. J., Ph, D., Mclaren, L. E. R. O. Y. C., Ph, D. & Hoyer, B. H. Enteroviral Ribonucleic Acid. **5010,** (1960).

4. Emini, E. a, Schleif, W. a, Colonno, R. J. & Wimmer, E. Antigenic conservation and divergence between the viral-specific proteins of poliovirus type 1 and various picornaviruses. *Virology* **140,** 13–20 (1985).

5. De Palma, A. M., Vliegen, I., De Clercq, E. & Neyts, J. Selective inhibitors of picornavirus replication. *Med. Res. Rev.* **28,** 823–884 (2008).

6. Norder, H. *et al.* Picornavirus non-structural proteins as targets for new anti-virals with broad activity. *Antiviral Res.* **89,** 204–218 (2011).

7. Gamarnik, A. V & Andino, R. Switch from translation to RNA replication in a positive-stranded RNA virus. 2293–2304 (1998). doi:10.1101/gad.12.15.2293

8. den Boon, J. a & Ahlquist, P. Organelle-like membrane compartmentalization of positive-strand RNA virus replication factories. *Annu. Rev. Microbiol.* **64,** 241–256 (2010).

9. Vignuzzi, M., Stone, J. K., Arnold, J. J., Cameron, C. E. & Andino, R. Quasispecies diversity determines pathogenesis through cooperative interactions in a viral population. *Nature* **439,** 344–348 (2006).

10. Vignuzzi, M., Wendt, E. & Andino, R. Engineering attenuated virus vaccines by controlling replication fidelity. *Nat. Med.* **14,** 154–161 (2008).

11. Gnadig, N. F. *et al.* Coxsackievirus B3 mutator strains are attenuated in vivo. *Proc. Natl. Acad. Sci.* **109,** E2294–E2303 (2012).

12. Xie, X. *et al.* Foot-and-mouth disease virus low-fidelity polymerase mutants are attenuated. *Arch. Virol.* **159,** 2641–2650 (2014).

13. Drake, J. W. A constant rate of spontaneous mutation in DNA-based microbes. *Proc. Natl. Acad. Sci. U. S. A.* **88,** 7160–7164 (1991).

14. Drake, J. W. & Holland, J. J. Mutation rates among RNA viruses. *Proc. Natl. Acad. Sci. U. S. A.* **96,** 13910–13913 (1999).

15. Korboukh, V. K. *et al.* RNA Virus Population Diversity, an Optimum for Maximal Fitness and Virulence. *J. Biol. Chem.* **289,** 29531–29544 (2014).

16. Ng, K. K. S., Arnold, J. J. & Cameron, C. E. Structure-function relationships among RNA-dependent RNA polymerases. *Current Topics in Microbiology and Immunology* **320,** 137–156 (2008).

17. Thibaut, H. J., De Palma, A. M. & Neyts, J. Combating enterovirus replication: State-of-the-art on antiviral research. *Biochem. Pharmacol.* **83,** 185–192 (2012).

18. Malet, H. *et al.* The flavivirus polymerase as a target for drug discovery. *Antiviral Res.* **80,** 23–35 (2008).

19. Ferrer-Orta, C., Ferrero, D. & Verdaguer, N. RNA-Dependent RNA Polymerases of Picornaviruses: From the Structure to Regulatory Mechanisms. *Viruses* **7,** 4438–4460 (2015).

20. Gong, P. & Peersen, O. B. Structural basis for active site closure by the poliovirus RNA-dependent RNA polymerase. *Proc. Natl. Acad. Sci. U. S. A.* **107,** 22505–22510 (2010).

21. Castro, C. *et al.* Nucleic acid polymerases use a general acid for nucleotidyl transfer. *Nat. Struct. & Mol. Biol.* **16,** 212–218 (2009).

22. Campagnola, G., Mcdonald, S. & Beaucourt, S. Structure-Function Relationships Underlying the Replication Fidelity of Viral RNA-dependent RNA Polymerases. **89,** 275–286 (2014).

23. Reilly, E. K. O., Kao, C. C. & O'Reilly, E. K. Analysis of RNA-dependent RNA polymerase structure and function as guided by known polymerase structures and computer predictions of secondary structure. *Virology* **303,** 287–303 (1998).

24. Liu, X. *et al.* Vaccine-derived Mutation in Motif D of Poliovirus RNA-dependent RNA Polymerase Lowers Nucleotide Incorporation Fidelity. *J. Biol. Chem.* **288,** 32753–32765 (2013).

25. Moustafa, I. M. *et al.* Structural Dynamics as a Contributor to Error-prone Replication by an RNA-dependent RNA Polymerase. *J. Biol. Chem.* **289,** 36229–36248 (2014).

26. Yang, X., Welch, J. L., Arnold, J. J. & Boehr, D. D. Long-Range Interaction Networks in the Function and Fidelity of Poliovirus RNA-Dependent RNA Polymerase Studied by Nuclear Magnetic Resonance. *Biochemistry* **49,** 9361–9371 (2010).

27. Yang, X. *et al.* Motif D of viral RNA-dependent RNA polymerases determines efficiency and fidelity of nucleotide addition. *Structure* **20,** 1519–1527 (2012).

28. Moustafa, I. M., Shen, H., Morton, B., Colina, C. M. & Cameron, C. E. Molecular Dynamics Simulations of Viral RNA Polymerases Link Conserved and Correlated Motions of Functional Elements to Fidelity. *J. Mol. Biol.* **410,** 159–181 (2011).

29. Campagnola, G., Weygandt, M., Scoggin, K. & Peersen, O. Crystal structure of coxsackievirus B3 3Dpol highlights the functional importance of residue 5 in picornavirus polymerases. *J. Virol.* **82,** 9458–9464 (2008).

30. Hobdey, S. E., Kempf, B. J., Steil, B. P., Barton, D. J. & Peersen, O. B. Poliovirus polymerase residue 5 plays a critical role in elongation complex stability. *J. Virol.* **84,** 8072–84 (2010).

31. Arnold, J. J. & Cameron, C. E. Poliovirus RNA-Dependent RNA Polymerase (3D p ol): Pre-Steady-State Kinetic Analysis of Ribonucleotide Incorporation in the Presence of Mg 2+ †. *Biochemistry* **43,** 5126–5137 (2004).

32. Gong, P., Kortus, M. G., Nix, J. C., Davis, R. E. & Peersen, O. B. Structures of Coxsackievirus , Rhinovirus , and Poliovirus Polymerase Elongation Complexes Solved by Engineering RNA Mediated Crystal Contacts. **8,** (2013).

33. Steitz, T. A. Visualizing polynucleotide polymerase machines at work. *EMBO J.* **25,** 3458–68 (2006).

34. Tzeng, S.-R. & Kalodimos, C. G. Protein dynamics and allostery: an NMR view. *Curr. Opin. Struct. Biol.* **21,** 62–67 (2011).

35. Graci, J. D. & Cameron, C. E. Challenges for the development of ribonucleoside analogues as inducers of error catastrophe. *Antivir. Chem. Chemother.* **15,** 1–13 (2004).

36. Hitomi, Y. *et al.* Inosine triphosphate protects against ribavirin-induced adenosine triphosphate loss by adenylosuccinate synthase function. *Gastroenterology* **140,** 1314–21 (2011).

37. Hansen, J. L., Long, a M. & Schultz, S. C. Structure of the RNA-dependent RNA polymerase of poliovirus. *Structure* **5,** 1109–1122 (1997).

38. Lyle, J. M., Bullitt, E., Bienz, K. & Kirkegaard, K. Visualization and functional analysis of RNA-dependent RNA polymerase lattices. *Science* **296,** 2218–22 (2002).

39. Wang, J., Lyle, J. M. & Bullitt, E. Surface for catalysis by poliovirus RNA-dependent RNA polymerase. *J. Mol. Biol.* **425,** 2529–2540 (2013).

40. Pathak, H. B. *et al.* Structure-function relationships of the RNA-dependent RNA polymerase from poliovirus (3Dpol). A surface of the primary oligomerization domain functions in capsid precursor processing and VPg uridylylation. *J. Biol. Chem.* **277,** 31551–62 (2002).

41. Boerner, J. E. *et al.* Allosteric Effects of Ligands and Mutations on Poliovirus RNA-Dependent RNA Polymerase Allosteric Effects of Ligands and Mutations on Poliovirus RNA-Dependent RNA Polymerase. *J. Virol.* **79,** 7803–7811 (2005).

42. Kati, W. M., Johnson, K. A., Jerva, L. F. & Anderson, K. S. Mechanism and fidelity of HIV reverse transcriptase. *J. Biol. Chem.* **267,** 25988–25997 (1992).

43. Cornish-Bowden, A. *Fundamentals of Enzyme Kinetics*. (Portland Press, 1995).

44. Gong, P., Campagnola, G. & Peersen, O. B. A quantitative stopped-flow fluorescence assay for measuring polymerase elongation rates. *Anal. Biochem.* **391,** 45–55 (2009).

45. Rachofsky, E. L., Osman, R. & Ross, J. B. A. Probing Structure and Dynamics of DNA with 2-Aminopurine: Effects of Local Environment on Fluorescence †. *Biochemistry* **40,** 946–956 (2001).

46. Joyce, C. M. Techniques used to study the DNA polymerase reaction pathway. *Biochim. Biophys. Acta* **1804,** 1032–40 (2010).

47. Dixon, M. The determination of enzyme inhibitor constants. *Biochem. J.* **55,** 170–171 (1953).

48. Cornish-Bowden, A. A simple graphical method for determining the inhibition constants of mixed, uncompetitive and non-competitive inhibitors. *Biochem. J.* **137,** 143–4 (1974).

49. Traut, T. W. Physiological concentrations of purines and pyrimidines. *Mol. Cell. Biochem.* **140,** 1–22 (1994).

50. Johnson, K. A., Simpson, Z. B. & Blom, T. Global kinetic explorer: a new computer program for dynamic simulation and fitting of kinetic data. *Anal. Biochem.* **387,** 20–9 (2009).

51. Johnson, K. A., Simpson, Z. B. & Blom, T. FitSpace explorer: an algorithm to evaluate multidimensional parameter space in fitting kinetic data. *Anal. Biochem.* **387,** 30–41 (2009).

52. Goodman, M. F., Creighton, S., Bloom, L. B. & Petruska, J. *Biochemical basis of DNA replication fidelity. Critical reviews in biochemistry and molecular biology* **28,** (1993).

53. Johnson, R. S. & Chester, R. E. UTP Allosterically Regulates Transcription by Escherichia coli RNA Polymerase from the Bacteriophage T7 A1 Promoter. *J. Mol. Biol.* **318,** 305–320 (2002).

54. Yokoyama, M., Mori, H. & Sato, H. Allosteric Regulation of HIV-1 Reverse Transcriptase by ATP for Nucleotide Selection. *PLoS One* **5,** e8867 (2010).

55. Lohmann, V., Overton, H. & Bartenschlager, R. Selective Stimulation of Hepatitis C Virus and Pestivirus NS5B RNA Polymerase Activity by GTP. *J. Biol. Chem.* **274,** 10807–10815 (1999).

56. Bressanelli, S., Tomei, L., Rey, F. A. & De Francesco, R. Structural analysis of the hepatitis C virus RNA polymerase in complex with ribonucleotides. *J. Virol.* **76,** 3482–92 (2002).

57. Cai, Z., Yi, M., Zhang, C. & Luo, G. Mutagenesis Analysis of the rGTP-Specific Binding Site of Hepatitis C Virus RNA-Dependent RNA Polymerase. *J Virol.* **79,** 11607–11617 (2005).

58. Sofia, M. J., Chang, W., Furman, P. A., Mosley, R. T. & Ross, B. S. Nucleoside, nucleotide, and non-nucleoside inhibitors of hepatitis C virus NS5B RNA-dependent RNA-polymerase. *J. Med. Chem.* **55,** 2481–531 (2012).

59. Feuer, R. & Whitton, J. L. Preferential coxsackievirus replication in proliferating/activated cells: implications for virus tropism, persistence, and pathogenesis. *Curr. Top. Microbiol. Immunol.* **323,** 149–73 (2008).

60. Dundas, J. *et al.* CASTp: computed atlas of surface topography of proteins with structural and topographical mapping of functionally annotated residues. *Nucleic Acids Res.* **34,** W116–W118 (2006).

61. Binkowski, T. A. CASTp: Computed Atlas of Surface Topography of proteins. *Nucleic Acids Res.* **31,** 3352–3355 (2003).

62. Panjkovich, A. & Daura, X. PARS: A web server for the prediction of Protein Allosteric and Regulatory Sites. *Bioinformatics* **30,** 1314–1315 (2014).

63. Hendlich, M., Rippmann, F. & Barnickel, G. LIGSITE: automatic and efficient detection of potential small molecule-binding sites in proteins. *J. Mol. Graph. Model.* **15,** 359–63, 389 (1997).

64. Huang, B. & Schroeder, M. LIGSITEcsc: predicting ligand binding sites using the Connolly surface and degree of conservation. *BMC Struct. Biol.* **6,** 19 (2006).

65. Morris, G. M. *et al.* AutoDock4 and AutoDockTools4: Automated docking with selective receptor flexibility. *J. Comput. Chem.* **30,** 2785–91 (2009).

66. Morin, A. *et al.* Collaboration gets the most out of software. *Elife* **2,** e01456 (2013).

67. Haudecoeur, R., Peuchmaur, M., Ahmed-Belkacem, A., Pawlotsky, J.-M. & Boumendjel, A. Structure-Activity Relationships in the Development of Allosteric Hepatitis C Virus RNA-Dependent RNA Polymerase Inhibitors: Ten Years of Research. *Med. Res. Rev.* **33,** 934–984 (2013).

68. Barreca, M. L., Iraci, N., Manfroni, G. & Cecchetti, V. Allosteric inhibition of the hepatitis C virus NS5B polymerase: in silico strategies for drug discovery and development. *Future Med. Chem.* **3,** 1027–55 (2011).

69. Mallalieu, N. L. *et al.* Pharmacokinetics and pharmacodynamics of setrobuvir, an orally administered hepatitis C virus non-nucleoside analogue inhibitor. *Clin. Ther.* **36,** 2047–2063.e3 (2014).

70. Boyce, S. E. *et al.* Structural and regulatory elements of HCV NS5B polymerase--β-loop and C-terminal tail--are required for activity of allosteric thumb site II inhibitors. *PLoS One* **9,** e84808 (2014).

71. Campagnola, G., Gong, P. & Peersen, O. B. High-throughput screening identification of poliovirus RNA-dependent RNA polymerase inhibitors. *Antiviral Res.* **91,** 241–51 (2011).

72. Sholders, A. J. & Peersen, O. B. Distinct conformations of a putative translocation element in poliovirus polymerase. *J. Mol. Biol.* **426,** 1407–1419 (2014).

73. Garriga, D., Ferrer-Orta, C., Querol-Audí, J., Oliva, B. & Verdaguer, N. Role of motif B loop in allosteric regulation of RNA-dependent RNA polymerization activity. *J. Mol. Biol.* **425,** 2279–2287 (2013).

74. Peersen, O. B., Pratt, E. A., Truong, H. T., Ho, C. & Rule, G. S. Site-specific incorporation of 5-fluorotryptophan as a probe of the structure and function of the membrane-bound D-lactate dehydrogenase of Escherichia coli: a 19F nuclear magnetic resonance study. *Biochemistry* **29,** 3256–62 (1990).